Current sheets in the heliosheath: Voyager 1, 2009

L. F. Burlaga[1] and N. F. Ness[2]

Received 22 November 2010; revised 18 January 2011; accepted 10 February 2011; published 10 May 2011.

[1] We identified all of the current sheets for which we have relatively complete and accurate magnetic field (**B**) data from Voyager 1 (V1) from days of year (DOYs) 1 to 331, 2009, which were obtained deep in the heliosheath between 108.5 and 111.8 AU. Three types of current sheets were found: (1) 15 proton boundary layers (PBLs), (2) 10 and 3 magnetic holes and magnetic humps, respectively, and (3) 3 sector boundaries. The magnetic field strength changes across PBL, and the profile B(t) is linearly related to the hyperbolic tangent function, but the direction of **B** does not change. For each of the three sector boundaries, **B** rotated in a plane normal to the minimum variance direction, and the component of **B** along the minimum variance direction was zero within the uncertainties, indicating that the sector boundaries were tangential discontinuities. The structure of the sector boundaries was not as simple as that for PBLs. The average thickness of magnetic holes and humps (~30 R_L) was twice that of the PBLs (~15 R_L). The average thickness of the current sheets associated with sector boundaries was close to the thickness of the PBLs. Our observations are consistent with the hypothesis that magnetic holes and humps are solitons, which are initiated by the mirror mode instability, and evolve by nonlinear kinetic plasma processes to pressure balanced structures maintained by magnetization currents and proton drift currents in the gradients of B.

Citation: Burlaga, L. F., and N. F. Ness (2011), Current sheets in the heliosheath: Voyager 1, 2009, *J. Geophys. Res.*, *116*, A05102, doi:10.1029/2010JA016309.

1. Introduction

[2] Voyager 1 (V1) and Voyager 2 (V2) crossed the termination shock and entered the heliosheath during December 2004 and August 2007, respectively [*Stone et al.*, 2005, 2008; *Burlaga et al.*, 2005, 2008]. In the heliosheath behind the termination shock, both V1 and V2 often observed a large change in the magnitude of **B** on a scale of several hours or less [see, e.g., *Burlaga et al.*, 2006a, 2006b]. In plots of 48 s averages of the magnetic field strength B, three types of profiles were observed: (1) those associated with proton boundary layers (PBLs), (2) magnetic holes and humps, and (3) sector boundaries. These structures are discussed in sections 2, 3, and 5, respectively. References to the earlier work on these structures are presented in sections 2, 3, and 5. Owing to the difficulty in separating the heliosheath signal from the noise and the systematic errors in the 48 s averages of **B**, only a few examples of these kinds of current sheets have been published. The aim of this paper is to describe all of the three types of current sheets listed above observed by V1 from day 1 through day 331, 2009 when V1 moved from 108.5 to 111.8 AU.

[3] Tangential discontinuities are a fundamental feature of the solar wind at 1 AU [see *Burlaga*, 1995, and references therein]. Current sheets associated with tangential discontinuities observed at 1 AU were discussed by *Burlaga et al.* [1977]. The magnetic field strength and/or direction can change across such a current sheet. The current sheets that we identified as PBLs in the V1 data for 2009 have no significant change in the magnetic field direction across the current sheets; thus, they are not rotational discontinuities. The magnitude of **B** increases or decreases across these PBLs, consistent with either tangential discontinuities or shocks. Section 5 shows that the PBLs are too thick to be shocks. Therefore, we infer that these current sheets are associated with tangential discontinuities. A theory of current sheets associated with tangential discontinuities, based on solutions to the Vlasov equations, was presented by the *Lemaire and Burlaga* [1976]. They identified two types of planar current sheets, "proton boundary layers" and "electron boundary layers," respectively. The thickness of the proton boundary layers and electron boundary layers is of the order of a few proton Larmor radii (R_L) and electron Larmor radii, respectively. No electron boundary layers were observed in a survey of 287 discontinuities at 1 AU [*Burlaga et al.*, 1977], and no electron boundary layers were identified in the heliosheath observations that we will discuss. The absence of electron boundary layers is consistent with the prediction of *Lemaire and Burlaga*

[1]Geospace Physics Laboratory, NASA Goddard Space Flight Center, Greenbelt, Maryland, USA.
[2]Institute for Astrophysics and Computational Sciences, Catholic University of America, Washington, D. C., USA.

Copyright 2011 by the American Geophysical Union.
0148-0227/11/2010JA016309

[1976] that these boundary layers would be unstable. The proton boundary layers are stable.

[4] Magnetic holes and humps have a three-part structure: an interval of uniform magnetic field strength B1, followed by a current sheet associated with a depression or enhancement of B, followed by another interval of uniform magnetic field strength B2. Magnetic holes and humps, like PBLs, need not be associated with a change in the magnetic field direction. There are several theories of magnetic holes and humps, which are referenced in section 3.

[5] Sector boundaries are a third kind of current sheet, necessarily associated with a large change in the direction of **B** which may or may not be associated with change in magnitude of **B**. Many people assume that a sector boundary is null sheet in which the magnetic field direction is constant, but B decreases to zero in the middle of the current sheet and then increases to its original value on the other side of the sheet with a change in sign. This configuration is rarely observed. Others assume that **B** rotates across sector boundary such a way that B remains constant but the direction of **B** changes by 180° [*Smith*, 2001]. In general the structure of the current sheet sector boundary is more complicated than this. The boundary between two sectors can be a single thin current sheet, multiple sheets, or a broad current sheet with a complex and even multifractal structure [*Klein and Burlaga*, 1980]. This paper considers three sector boundaries in the heliosheath which all appear to be a part of the transition from one sector to another sector of the opposite polarity.

2. Current Sheets Associated With Proton Boundary Layers

2.1. The Kinetic Theory of Proton Boundary Layers

[6] In the kinetic theory of proton boundary layers introduced by *Lemaire and Burlaga* [1976] the electron distribution function is the sum of two electron Maxwellians whose relative concentrations change smoothly across the current sheet Maxwellian, and the proton distribution function is the sum of two truncated anisotropic Maxwellians. The density N, proton temperature T and magnetic field **B**, change across the boundary layer from one state to another, but the electron temperature is constant. A changing density and the gyration of protons in the inhomogeneous magnetic field produce a charge separation that supports a small polarization electric field, which is larger for a larger density change, giving a thinner PBL when the density changes across the PBL is larger. The total pressure (the sum of the thermal, magnetic, and electric pressures) is constant across a PBL. The tail of a non-Maxwellian proton distribution within the PBL provides diamagnetic currents parallel to the PBL which is associated with the changes in **B**.

2.2. The Magnetic Field Strength Profile in a PBL

[7] Most of the tangential discontinuities observed in the solar wind near 1 AU are associated with a change in the direction of **B**, and little or no change in the magnitude of **B**. The heliosheath observations that we discuss below show primarily changes in B, with little or no change in the direction of **B**. There is an interval with nearly constant B = B1 and a smooth transition to another interval with constant B = B2 ≠ B1. We shall show that the magnetic field profile in the intermediate region has the form of the hyperbolic tangent function. The overall magnetic field strength profiles of the PBLs that convected past V1 during 2009 can be fit with the function

$$B(t) = (B1 + B2)/2 + [(B2 - B1)/2]\tanh[(t - t_0)/\tau] \qquad (1)$$

For early times, $t \ll t_0$, the hyperbolic tangent is −1 and B(t) = B1 > 0; for large times, $t \gg t_0$, the hyperbolic tangent is +1 and B(t) = B2 > 0.

[8] In practice, it is more efficient to use the sigmoid function to fit the magnetic field strength profile, which is equivalent to (1), but it involves the exponential function rather than the hyperbolic tangent. The sigmoid function is more suitable for a nonlinear curve fitting scheme based on the Levenberg-Marquardt algorithm [*Levenberg*, 1944; *Marquardt*, 1963]. The sigmoid function is defined as

$$y(x) = A2 + \{A1 - A2\}/\{1 + \exp[(x - x0)/dx]\} \qquad (2)$$

where A1 and A2 are asymptotic values of y, x0 is the inflection point, and dx measures the width of the change in y along the x direction.

[9] Changing the notation so that this formula applies to the specific problem at hand, we write (2) as

$$B(t) = B2 + \{B1 - B2\}/\{1 + \exp[(t - t_o)/\tau]\} \qquad (3)$$

where t will be plotted in units of days, τ is related to the width of the structure, and t_o is the time that the middle of the current sheet (the inflection point of B(t), where $B(t_o)$ = (B1 + B2)/2) moves past V1. The equivalence between (1) and (3) can be demonstrated after some algebra using the relationship $\tanh(z) = (e^z - 1)/(e^z + 1)$, where e^z is the exponential function exp(z).

[10] Since (1) and (3) approach B1 and B2 only asymptotically, it is necessary to define a reasonable "width" of the current sheet, "w" = $t_2 - t_1$ which is related to τ. This width w is a measure of the time for the current sheet to move past V1. Let us write $B(t_2) = B2 - \varepsilon(t_2)$. We choose t_2 such that $\varepsilon(t_2)$ is 10% of {B2 − B1}, i.e., $\varepsilon(t_2) \equiv -\{B1 - B2\}/\{1 + \exp(t_2 - t_o)/\tau]\} = 0.1\{B2 - B1\}$, which gives $10 = \{1 + \exp[(t_2 - t_o)/\tau]\}$ or $9 = \exp(t_2 - t_o)/\tau]\}$. Taking the natural logarithm of both sides gives $2.197 = (t_2 - t_0)/\tau$, or $\tau = (t_2 - t_0)/2.197$. Taking $w = 2 \times (t_2 - t_0)$ (since $(t_0 - t_1) = (t_2 - t_0)$), we obtain w (day) = 2 × 2.197 × τ (day), or w = 4.4 τ (day).

2.3. Identification of PBLs in the V1 2009 Observations

[11] We searched the plots of 48 s averages V1 observations of B(t) from day of year (DOY) 1 to 331.0, 2009 for profiles resembling those expected for current sheets associated with tangential discontinuities, PBLs. Fifteen events were identified unambiguously. Since the 1 σ uncertainty in B is typically ±0.03 nT for observations discussed in this paper, we cannot unambiguously identify PBLs with |B2 − B 1| < 0.05 nT. The smallest value of |B2 − B1| among the PBLs that we selected is |0.03 − 0.10| = 0.07 nT. Owing to the data gaps, primarily because of the limited tracking of the telemetry but also owing to various sources of noise, we have measurements for ~4230 h from DOY 1 to 331.0, i.e., 53% of the time. Fifteen PBLs were identified in this interval. The rate of observations of PBLs is 0.086/d, or 1 every 11.8 days.

Table 1. Proton Boundary Layers[a]

Event	t_o (DOY)	dt_o (days)	R^2	B1 (nT)	dB1 (nT)	B2 (nT)	dB2 (nT)	τ (days)	dτ (days)	w (h)	dw (h)	B2/B1
1	2.8349	0.0005	0.938	0.0147	0.0009	0.0704	0.0005	0.0045	0.0004	0.48	0.04	4.8
2	4.074	0.0010	0.821	0.0818	0.0003	0.1116	0.0005	0.0059	0.0008	0.62	0.08	1.36
3	11.815	0.0013	0.903	0.0514	0.0004	0.095	0.0003	0.0167	0.0012	1.76	0.13	1.85
4	46.5488	0.0006	0.951	0.1206	0.0005	0.0568	0.0007	0.0081	0.0054	0.86	0.57	0.47
5	47.5816	0.0008	0.901	0.0772	0.0005	0.1203	0.0006	0.0071	0.0007	0.75	0.07	1.56
6	72.7789	0.0013	0.909	0.1126	0.0005	0.1654	0.0007	0.0183	0.0012	1.93	0.13	1.47
7	102.4128	0.0017	0.750	0.0696	0.0006	0.0474	0.0006	0.0089	0.0015	0.94	0.16	0.68
8	126.6563	0.0036	0.884	0.1255	0.0037	0.0685	0.0006	0.0210	0.0023	2.22	0.24	0.55
9	128.4157	0.0021	0.927	0.115	0.0008	0.0456	0.0021	0.0443	0.0019	4.68	0.20	0.40
10	132.5215	0.0007	0.976	0.0482	0.0005	0.1582	0.0005	0.021	0.0006	2.22	0.06	3.28
11	140.5656	0.0006	0.977	0.1586	0.0004	0.0507	0.0004	0.0121	0.0005	1.28	0.05	0.32
12	157.8103	0.0017	0.871	0.1112	0.0006	0.0687	0.0005	0.0201	0.0015	2.12	0.16	0.62
13	167.5955	0.0017	0.865	0.0819	0.0004	0.0407	0.0005	0.0211	0.0015	2.23	0.16	0.50
14	211.659	0.0013	0.943	0.0997	0.0003	0.0281	0.0005	0.0334	0.0011	3.53	0.12	0.28
15	255.2059	0.0007	0.980	0.1058	0.0012	0.2851	0.0014	0.0150	0.0006	1.58	0.06	2.69

[a]See the auxiliary material for figures of events not shown in the main text. DOY, day of year.

[12] Among the 15 candidate PBLs that were identified, the data were incomplete for 5 of these events, which were observed on DOY 11, 102, 126, 128, and 211, 2009. Nevertheless, we were able to obtain good fits of the data with the function (2). Therefore, we include all of the events in the discussion of the statistics of the properties of the PBLs in section 4. We shall show plots of the data only for 4 of these 15 events. Plots of the remaining events are available in the auxiliary material.[1] The parameters for all of the PBLs are collected in Table 1.

2.4. Observations of the PBLs

[13] In this section we discuss the detailed profiles of four events that illustrate the fundamental characteristics of the observations of PBLs. When interpreting plots of Voyager magnetic field observations in the heliosheath and distant heliosphere it is essential to consider the effects of the uncertainties in the measurements of **B**. Typically the uncertainty in each component of **B** is ±0.02 nT and the uncertainty in B is 0.03 nT. We begin with an example of an exceptional event that shows both the basic features of the magnetic field profile B(t) in the PBLs and the effect of the uncertainties in the measurements of the direction of **B** when B is very small (Figure 1).

[14] The basic features of the PBL in Figure 1 are (1) a region of nearly uniform magnetic field strength B1, (2) a current sheet with an inflection in B(t) at the center of the sheet, followed by (3) a region with a different uniform magnetic field strength B2. The sigmoid function provides an excellent fit to the observations, $R^2 = 0.94$, where is R^2 is the coefficient of determination. The inflection point of B(t) moved past V1 at t_0 = DOY 2.8349 ± 0.0005, 2009. The initial and final magnetic field strengths derived from this fit are B1 = 0.0147 ± 0.0009 nT and B2 = 0.0704 ± 0.0005 nT, respectively, giving a relatively large jump B2/B1 = 4.8. The width of the current sheet as defined above is w = 0.48 ± 0.04 h. All of these numbers describing this event ("event 1") are given in Table 1. The uncertainties derived from the fit to the data should not be confused with the uncertainties in the measurements. In the following, we shall give the magnetic field strength to two or three significant figures, since the uncertainty in measurements of B is ±0.03 nT. The direction of **B**, given by the azimuthal and elevation angles λ and δ, respectively, is nearly constant

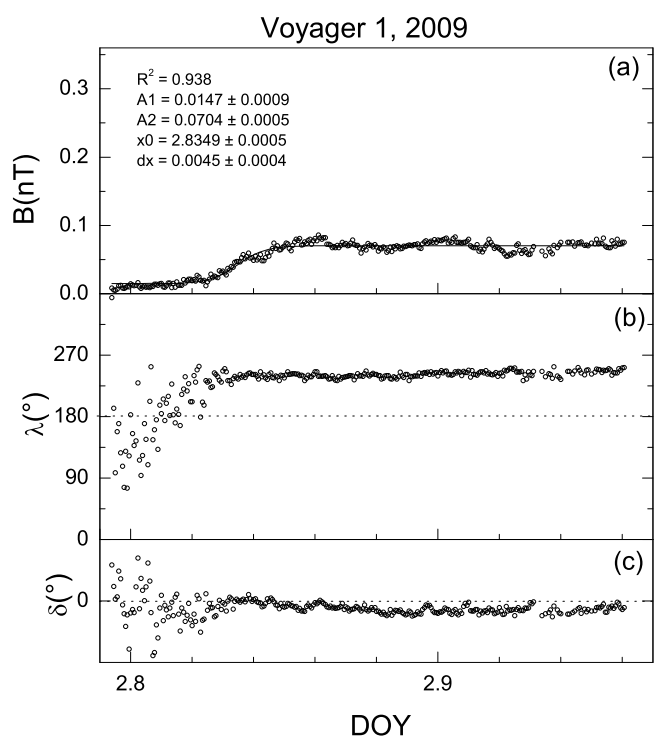

Figure 1. Voyager 1 observations of (a) the magnetic field strength B, (b) the azimuthal angle λ, and (c) the elevation angle δ for a tangential discontinuity (PBL) in which the current sheet between the two asymptotic values of B is resolved. The magnetic field strength at early times is BX = 0.015 nT, which is comparable to the uncertainty of B (±0.03 nT). Owing to these weak magnetic fields, the direction of **B** cannot be determined accurately. Apparent variations of λ and δ are consequences of the systematic and random errors. The solid curve in Figure 1a is a least squares fit of the sigmoid function (2) to the data; the parameters of this fit are also shown in Figure 1a.

[1]Auxiliary materials are available in the HTML. doi:10.1029/2010JA016309.

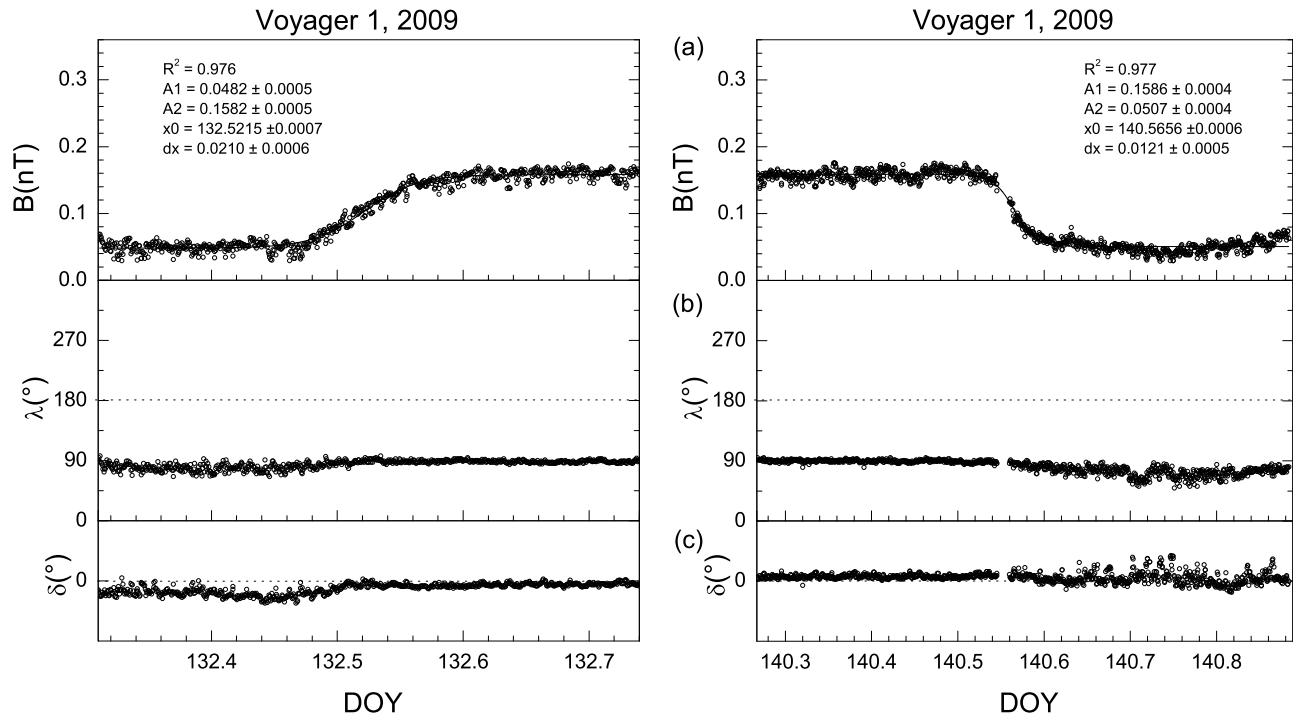

Figure 2. Observations of two PBLs with relatively large changes in B, plotted in the format of Figure 1. (left) The observations show an increase in B; (right) the observations show a decrease in B. The direction of the magnetic field across both PBLs is constant and in the direction of the Parker spiral (λ = 90°/270° and δ = 0°) within the uncertainties of the measurements.

across most of the PBL in Figure 1, but the scatter is very large, and the angles are essentially meaningless in the region ahead of the current sheet (where the average B derived from the fit is only 0.015 nT) because the uncertainties in the measurements of each component of **B** are of the order of ±0.02 nT. For such weak magnetic fields, the measured signal is dominated by the systematic and random errors in the measurements.

[15] In general, the measured magnetic field strength is the sum of two signals: the physical signal produced by the heliosheath magnetic field, and the "error" signal produced by the systematic and random uncertainties. When B is weak, the error signal is dominant; when B is strong, the heliosheath magnetic field is dominant. Between these extremes both signals must be considered in the interpretation of the data.

[16] Two more typical PBLs, with B1 and B2 closer to the average magnetic field strength in the data ($\langle B \rangle$) = 0.01 nT), are shown in Figure 2. Figure 2a shows a PBL in which B increases as it moves past V1 (a "positive jump"), and Figure 2b shows a PBL in which B decreases as it moves past V1 (a "negative jump"). The curves in Figure 2a and 2b are best fits to the sigmoid function (2), which are equivalent to fits of the hyperbolic tangent function (1). The sigmoid function provides an excellent fit to the data in both cases. The parameters describing the observations and fits for these events (events 10 and 11, respectively) are given in Table 1. Note that for both events where B is relatively low, ~0.05 nT, (1) the scatter of the measurements of the angles λ and δ increases and (2) there is a small change in the trend of the angles in the regions. These two effects are a consequence of both systematic and statistical uncertainties in the measurements of **B**, respectively. Within the uncertainties of the measurements, there is no change in direction across either of these PBLs.

[17] Finally, we discuss a remarkable PBL (event 15 in Table 1), shown in Figures 3a–3c. The sigmoid function provides an excellent fit to B (t). The current sheet moved past at V1 at t_0 = DOY 255.2059, 2009. The magnetic field strength increased across the current sheet from 0.11 nT to the large value 0.29 nT (B2/B1 = 2.69). The magnetic field direction is nearly constant. Both large-scale and small-scale variations in the direction of **B** occur where the field is relatively weak, but still close to the mean heliosheath magnetic field strength, ~0.1 nT. This current sheet is a very distinct boundary of a large region with very strong heliosheath magnetic fields (reaching 0.35 nT) shown in Figure 3d. This unusual region [*Burlaga and Ness*, 2010] continued to move past V1 for at least 20 days. The nature and origin of this region are unknown.

3. Magnetic Holes and Humps

3.1. Introduction

[18] The magnetic field is a vector field, and points where **B** = 0 in a vector field are of special interest because the magnetic topology can change at these points. For example, *Burlaga* [1968] and *Burlaga and Ness* [1969] identified microscale structures in the solar wind at 1 AU where B was close to zero and the magnetic field direction changed significantly. They suggested that these "D sheets" might be sites of magnetic reconnection. No D sheets were observed in the V1 data from DOY 1 to 331, 2009. There is no

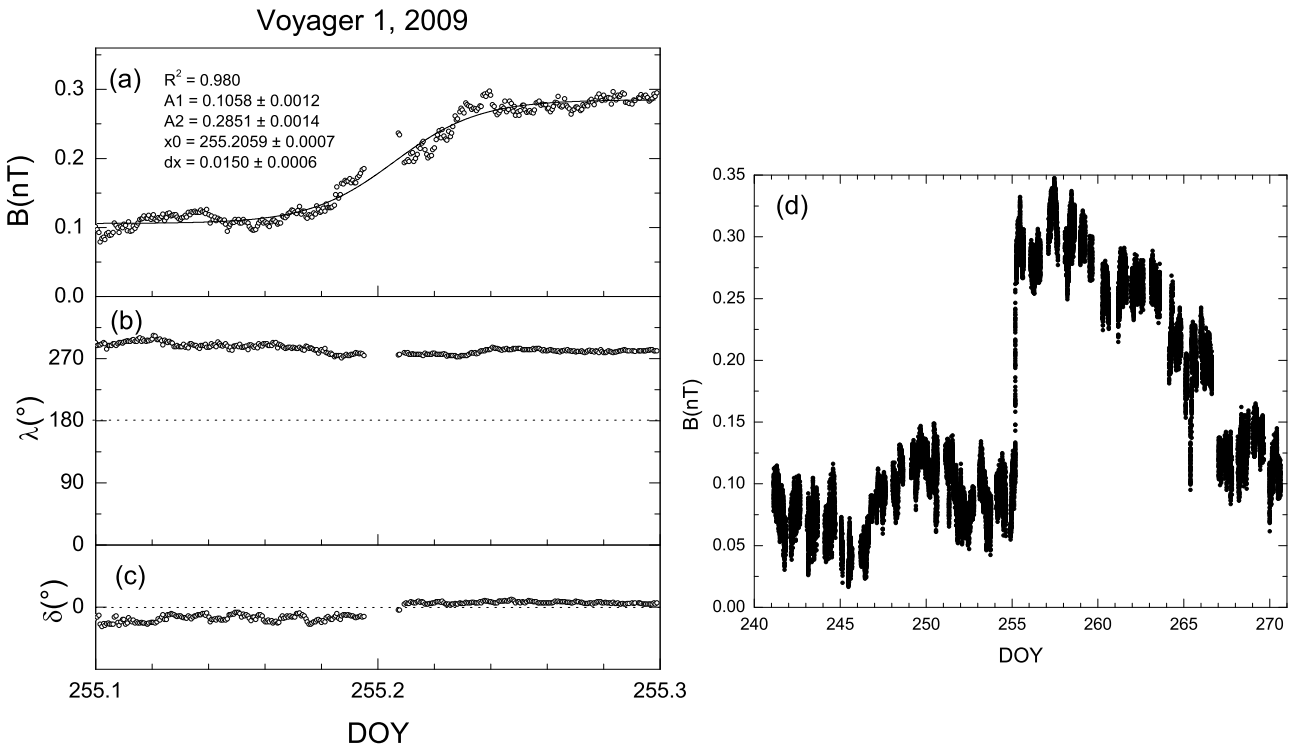

Figure 3. (a–c) Observations of a PBL with a large change in B. The direction of the magnetic field was nearly constant across this current sheet, in the direction of the Parker spiral direction (λ = 270° and δ = 0°). (d) This current sheet formed the front boundary of an unusual region with very intense magnetic fields that persisted for at least 20 days.

evidence of magnetic reconnection in the V1 data set discussed in this paper.

[19] A search for small regions in the solar wind with B < 1 nT in plots of 15 s magnetic field averages of **B** from Explorer 43 at 1 AU revealed the existence of another type of magnetic structure with weak magnetic fields, called "magnetic holes" [*Turner et al.*, 1977]. Twenty-eight magnetic holes were observed during in the 19 day interval corresponding to the rate of 1.5 magnetic holes per day. None of these magnetic holes had B = 0. Some (but not all) of these magnetic holes were not associated with a change in the magnetic field direction ("linear magnetic holes"), and are therefore not related to magnetic reconnection. Similar structures, with an enhancement of B rather than depression (now called "magnetic humps") and no change in the magnetic field direction were also discovered by *Turner et al.* [1977].

[20] Magnetic holes are observed throughout the solar wind. Further studies of magnetic holes in the solar wind at 1 AU were published by [*Fitzenreiter and Burlaga*, 1978; *King et al.*, 1979; *Stevens and Kasper*, 2007]. Magnetic holes were also observed in the region out of the ecliptic in data from Ulysses [*Neugebauer et al.*, 2001; *Tsurutani et al.*, 2002; *Winterhalter et al.*, 1994a, 1994b, 2000] and in the supersonic solar wind out to 17 AU [*Sperveslage et al.*, 2000].

[21] Magnetic holes have also been observed in the magnetosheath of Earth [*Constantinescu et al.*, 2003; *Horbury et al.*, 2004; *Soucek et al.*, 2008; *Stasiewicz et al.*, 2003; *Tátrallyay and Erdös*, 2002, 2005], Jupiter [*Erdös and Balogh*, 1996; *Joy et al.*, 2006], and Saturn [*Bavassano Cattaneo et al.*, 1998].

[22] A kinetic theory of magnetic holes and magnetic humps was published by *Burlaga and Lemaire* [1978] based on the following assumptions: (1) They are stationary (nonpropagating) structures convected with the solar wind. (2) They are locally planar structures whose curvature is large compared to the thickness (which is supported by observations discussed by *Fitzenreiter and Burlaga* [1978]); the magnetic field direction is parallel to the plane of the structures and its magnitude varies along the direction orthogonal to the plane. (3) The plasma is collisionless. (4) The current is the sum of the gradient drift current and the magnetization current of the protons moving in the gradients of the magnetic field and plasma. It was concluded, based on a solution of the Vlasov equation, that magnetic holes and humps are pressure balanced structures.

[23] Another hypothesis concerning the nature of magnetic holes and humps was offered by *Tsurutani et al.* [1992], who suggested that they are mirror mode waves produced by the linear mirror mode instability, driven by temperature anisotropy of the plasma. The "mirror mode" is a long-wavelength, nonpropagating mode, which is different than the three basic MHD modes. *Southwood and Kivelson* [1993], expanding on the early work of *Tajiri* [1967] and *Hasegawa* [1969], showed that even in the linear limit, the mirror mode instability should be treated with kinetic theory and include finite Larmor radius corrections. It is difficult to test the hypothesis of Tsurutani, because even today there is no agreement on the nature of

the structures that result from the nonlinear development of the mirror mode instability. There is a large literature on the theory of the mirror mode instability, which we will not review here. The nonlinear theory, with finite Larmor radius effects and non-Maxwellian distributions, is particularly important [e.g., *Kivelson and Southwood*, 1996; *Pantellini*, 1998; *Génot et al.*, 2001; *Pokhotelov et al.*, 2004, 2008; *Istomin et al.*, 2009]. It is generally found that the quasi-stationary nonlinear structure that eventually develops from the mirror instability is a pressure balanced structure.

[24] A fundamental difference between the two theories of magnetic holes and humps just described is in the geometry. *Burlaga and Lemaire* [1978] assumed a planar structure, with variations perpendicular to the magnetic field direction and the plane of the current sheet, but no variation along the magnetic field direction. In contrast, the mirror mode requires variations along the magnetic field direction, which is presumed to have a sausage-like shape.

[25] A third theory [*Baumgärtel*, 1999; *Baumgärtel et al.*, 2005] is that magnetic holes and humps are solitons. (The magnetic holes and humps that we consider are different than the isolated very small scale features, 30 ion skin lengths, identified by *Rees et al.* [2006] and modeled as "banana-polarized solitons" by *Sauer et al.* [2007] and *Baumgärtel et al.* [2007].) It is commonly assumed that solitons are necessarily fluid structures, such as the solitons introduced by *Korteweg and de Vries* [1895] and *Lamb* [1980]. *Baumgärtel et al.* [1997] and others argued that Hall MHD can provide the dispersive effects necessary for a soliton. On the other hand, it seems clear that the finite Larmor radius effect must be considered [e.g., *Hall*, 1979; *Pokhotelov et al.*, 2004], and this too can produce the dispersive effects required for solitons. Kinetic theories [e.g., *Istomin et al.*, 2009] show it is possible that solitons can form from the nonlinear evolution of the mirror mode instability in plasmas.

[26] There is a widespread belief that the linear mirror mode instability is the cause of magnetic holes and magnetic humps, and that this theory is not consistent with theories of solitons and pressure balanced structures. However, we offer the hypothesis that all three of the theories discussed above are relevant to understanding magnetic holes and humps. For example, the linear mirror mode instability driven by temperature anisotropy might be the initial cause of the initial development of these structures. The fully nonlinear development the mirror mode instability in non-Maxwellian plasmas with finite Larmor radius effects might produce solitons (and other structures). And the fully developed nonlinear structures are likely to be pressure balanced structures.

[27] Ideally, one should have observations from two points suitably placed along the magnetic field direction in order to distinguish between magnetic holes and magnetic humps, as well as high-resolution observations of the distribution functions of particles and fields. In the V1 observations, this is not possible. Consequently, the emphasis in this paper is on the description of the observations of the magnetic field profiles associated with magnetic holes and magnetic humps observed by V1 in the heliosheath.

[28] The existence of magnetic holes in heliosheath was demonstrated by *Burlaga et al.* [2006a]. The existence of trains of magnetic holes and magnetic humps in the heliosheath was demonstrated by *Burlaga et al.* [2006b], who showed that the profiles B(t) are approximately Gaussian distributions. These authors could not determine whether magnetic holes and humps are mirror mode structures, solitons or pressure balanced structures in the Voyager data. Nine isolated magnetic holes in the V1 data were studied by *Burlaga et al.* [2007], who showed that the average width (passage time) of the magnetic holes was 2.3 h with the standard deviation of 0.7 h.

[29] Further observations of magnetic holes in the V1 data obtained in the heliosheath were published by *Tsurutani et al.* [2011], who interpreted them in terms of the mirror mode instability, although conclusive evidence in support this interpretation was not given. *Liu et al.* [2006] and *Génot* [2008] suggested that the heliosheath plasma behind the termination shock should be unstable to the mirror instability and proposed that magnetic holes and magnetic humps are different stages of the mirror instability. However, these papers do not consider the pickup protons, which would provide the dominant contribution to the temperature anisotropy that drives the mirror mode instability in the heliosheath.

[30] In the distant heliosphere and heliosheath, pickup protons provide the dominant contribution to the thermal pressure [*Burlaga et al.*, 1996], and they will likely determine the thickness and structure of the magnetic holes and humps. A theory of solitons, including the effects of pickup protons, was presented by *Avinash and Zank* [2007] and *Avinash et al.* [2009]. This theory explains the magnetic field strength profiles of the magnetic holes observed in the heliosheath.

3.2. Identification and Fitting Function of Magnetic Holes in the Heliosheath by V1 During 2009

[31] We searched the V1 observations of B from DOY 1 to 331.0, 2009 for profiles B(t) resembling those expected for magnetic holes and magnetic humps. Ten candidate magnetic holes and three candidate magnetic humps were identified (events 1–15 in Table 2). In all cases only a part of the magnetic hole or magnetic hump was observed, owing to gaps in the data. These gaps are the result of various sources: limited tracking of the spacecraft (~6–12 h/d); poor quality of the ground station reception when the viewing angle is near the horizon; noise from the instrument, the spacecraft and the telemetry system; operations such as rolls and calibrations, etc. The data used in this study were carefully edited by hand using all the information available.

[32] Following *Burlaga et al.* [2006b] for the sake of comparison, we fit each event empirically to a Gaussian distribution $y = y0 + A/[w \times \sqrt{(\pi/2)}] \times \exp\{-2 \times [(x - xc)/w]^2)\}$. With the symbols that were used in the definition of the sigmoid function (3), the relevant form of the Gaussian distribution is

$$B = B0 + A/[\tau\sqrt{(\pi/2)}] \times \exp\left\{-2 \times [(t - t_0)/\tau]^2\right\} \quad (4)$$

where $\tau = 2\sigma$, σ is the standard deviation, and A is the parameter in the Gaussian distribution for y(x). The parameter τ is the distance between the two inflection points of the Gaussian distribution, which accounts for 68.2% of the area under the Gaussian distribution. Intuitively, the "width" of the distribution appears to be broader than the

Table 2. Magnetic Holes (Events 1–10) and Magnetic Humps (Events 11–13)[a]

Event	t_o (DOY)	dt_o (days)	R^2	B0	dB0	A	dA0	τ (days)	$d\tau$ (days)	w (h)	dw (h)	Bm	Bm/B0	BM	BM/B0
1	52.936	0.0009	0.932	0.1027	0.0004	−0.0093	0.0002	0.1177	0.0021	2.82	0.05	0.04	0.39		
2	77.8596	0.0008	0.781	0.1300	-	−0.0131	0.0002	0.1394	0.0024	3.35	0.06	0.06	0.42		
3	78.6417	0.0010	0.737	0.0389	0.0005	−0.0021	0.0001	0.0761	0.0010	1.83	0.02	0.02	0.43		
4	124.3981	0.0009	0.948	0.1333	0.0009	−0.0259	0.0005	0.2357	0.0032	5.66	0.08	0.05	0.34		
5	137.6699	0.0007	0.905	0.1244	0.0029	−0.0171	0.0011	0.1566	0.0052	3.76	0.12	0.04	0.30		
6	162.7729	0.0013	0.812	0.0910	0.0004	−0.0119	0.0002	0.1553	0.0030	3.73	0.07	0.03	0.33		
7	196.401	0.0008	0.896	0.1300	-	−0.0222	0.0002	0.1804	0.0018	4.33	0.04	0.03	0.24		
8	201.5027	0.0006	0.904	0.1430	0.0004	−0.0020	0.0001	0.0374	0.0006	0.90	0.01	0.10	0.70		
9	201.8208	0.0004	0.936	0.1359	0.0005	−0.0048	0.0001	0.0562	0.0010	1.35	0.02	0.07	0.50		
10	236.6669	0.0006	0.949	0.1163	0.0006	−0.0099	0.0002	0.0951	0.0016	2.28	0.04	0.03	0.29		
11	151.8781	0.0007	0.937	0.0281	0.0007	0.0185	0.0004	0.1840	0.0025	4.42	0.06			0.11	3.85
12	308.1067	0.0017	0.559	0.1163	0.0006	0.0071	0.0003	0.1061	0.0038	2.55	0.09			0.17	1.46
13	103.6154	0.0008	0.9233	-	0.0000	0.0794	0.0003	0.4166	0.0022	10.00	0.05		-	0.15	-

[a]See the auxiliary material for figures of events not shown in the main text.

distance between inflection points. We define the "width" (passage time) of the magnetic hole or hump as w′: = 2 τ. This definition is consistent with our definition of the width of a PBL in section 2. The minimum or maximum magnetic field strength (Bm or BM, in the magnetic holes and magnetic humps, respectively) occur at t = t_0, when

$$B = B0 + A/[\tau \times \sqrt{(\pi/2)}] \quad (5)$$

where A > 0 for a magnetic hump and A < 0 for a magnetic hole. The Gaussian distribution does not have a physical basis in theory of magnetic holes and magnetic humps. However, the model of *Avinash and Zank* [2007] provides a profile that is close to the Gaussian distribution. In some cases, one observes a sharper edge of the magnetic hole or hump than is described by the Gaussian distribution; such a sharp edge does appear some solutions in the model of *Burlaga and Lemaire* [1978]. In any case, the accuracy of the fit of the Gaussian function to the observations can be specified, and the parameters derived from a Gaussian fit are characteristic of the magnetic holes and humps. Deviations of the shapes of magnetic holes and magnetic humps from the Gaussian distribution provide insight into their detailed structure. We would obtain the best fits to the data with the Gaussian distribution if the data set were continuous, beginning with an interval of constant magnetic field (B0), followed by a magnetic hole or hump, and ending with another interval of constant magnetic field (B0). However,

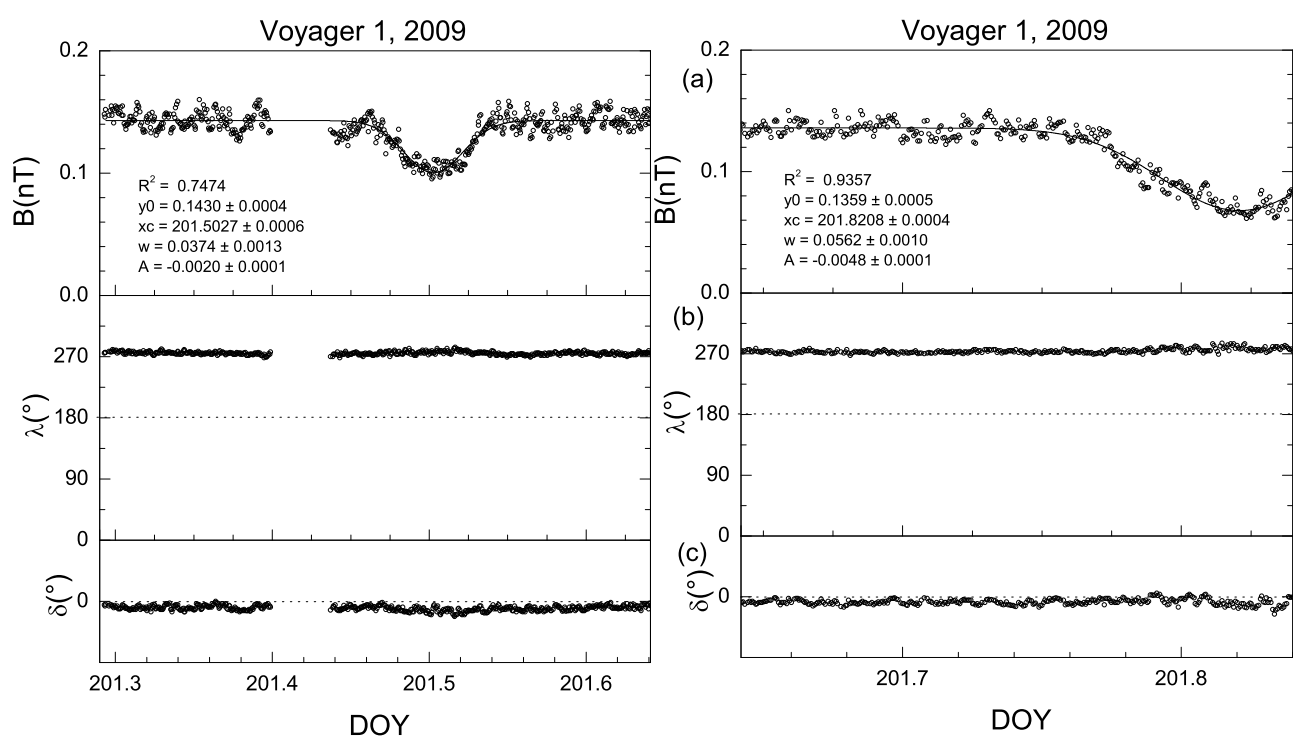

Figure 4. Observations of two magnetic holes. The azimuthal angle and elevation angle of **B** magnetic field direction are constant (λ = 270° and δ = 0°, respectively, along the Parker spiral direction) across the both magnetic holes. The solid curves in Figure 4a are fits to the Gaussian distribution in equation (3). The parameters of the respective fits are also plotted.

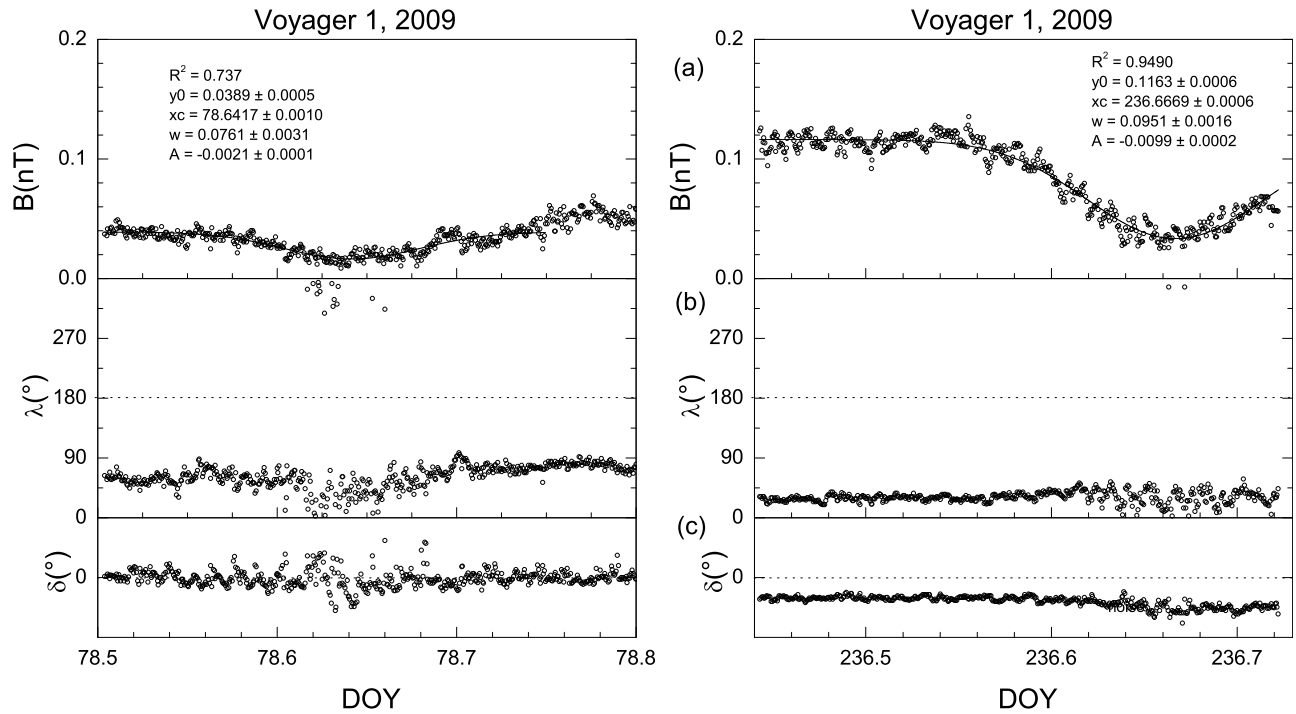

Figure 5. Observations of two magnetic holes in the same format described in the caption of Figure 4. (left) Owing to the weak magnetic fields, the effects of systematic and random uncertainties in the angles are relatively large, but the data are consistent with a constant magnetic field direction across the magnetic hole. (right) The angles of **B** differ appreciably from the Parker direction, but the direction is constant across the magnetic hole within the uncertainties.

we have not observed all three parts of the profile in any of the events in the data set under consideration, primarily owing to limited tracking of the telemetry signal from V1.

[33] We present a summary of the parameters of all of the events identified in the V1 2009 data set in Table 2. We found significantly more magnetic holes than magnetic humps, the ratio being at least $10/3 \approx 3$. This ratio could be a result of different production rates and/or different decay rates of the structures. In any case, this ratio provides a constraint on the mechanism that forms magnetic holes and humps, such as the mirror mode instability. Section 3.3 illustrates the properties of magnetic holes for a representative sample of the events in the data set.

3.3. Observations of the Magnetic Holes and Humps

[34] Figure 4 shows two magnetic holes that happened to move past V1 on the same day: event 8 at t_0 = DOY 201.5027 (Figure 4, left), and event 9 at t_0 = DOY 201.8208 (Figure 4, right), respectively. As in the plots of PBLs in section 2, the length of the abscissa is the same in both Figures 4 (left) and 4 (right), and the timescale in Figures 4, 5 and 6 is the same, with major ticks at 0.1 day intervals. Since the time intervals in each plot are chosen to show the largest set of nearly continuous data, the length of a 0.1 day interval will not be the same in every plot. All of the plots have the same ordinate, for the sake of comparing the magnitudes of **B**.

[35] Event 8 has the most complete coverage of the events that we observed, although there is still a small data gap. One can see all three parts of the magnetic hole: the entire depression of B(t) (which can be modeled as two adjacent PBLs); an extended region of nearly constant B before the depression; and an extended region with the same magnetic field strength B = B0 after the depression. The minimum B in the depression is Bm = 0.10 nT and B0 = 0.14 nT, giving Bm/B0 = 0.70. The Gaussian distribution, shown by the solid curve in Figure 4, provides a good fit to the data $R^2 = 0.904$. The width of the magnetic hole, $w = 2\tau$, is dw = 0.90 ± 0.01 h. These parameters for this event (event 8) are summarized in Table 2. The direction of **B** is constant throughout the interval.

[36] The data for the event 9, shown in Figure 4 (right) are incomplete; the data for most of the second part of the magnetic depression and the constant magnetic field region following the magnetic depression are missing. Nevertheless, one can fit the data with a Gaussian distribution, assuming that B before the magnetic depression is equal to that after the magnetic depression. An excellent fit, with $R^2 = 0.936$, is shown by the solid curve in Figure 4. The width of the magnetic hole is w = 1.35 ± 0.02 h. The minimum B in the depression is Bm = 0.07 nT and B0 = 0.14 nT, giving Bm/B0 = 0.50. A slight deviation in the direction of **B** is observed as B decreases in the magnetic hole, but this deviation is due to the systematic errors, which manifest themselves when B is weak. The direction of **B** is nearly constant across the entire interval within the uncertainties.

[37] Another pair of magnetic holes is shown in Figure 5 whose midpoints moved past V1 at t_o = DOY 78.6417 (Figure 5, left, event 3) and DOY 236.6669 (Figure 5, right,

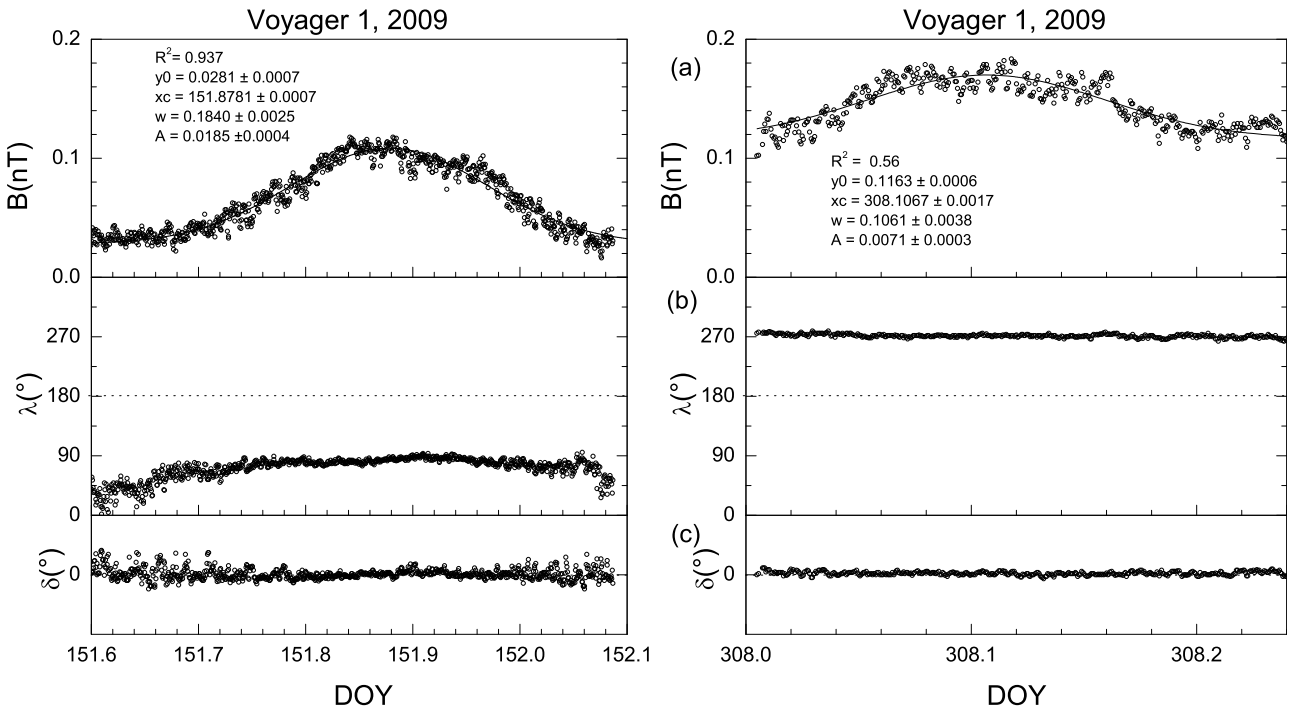

Figure 6. Observations of two magnetic humps in the same format as the data in Figure 4. The magnetic field direction is constant within the uncertainties (λ = 90° and δ = 0°, along the Parker spiral direction) across the both magnetic humps. The solid curves in Figure 6a are fits to the Gaussian distribution (equation (4)).

event 10), respectively. In event 3, the depression in the magnetic hole is well defined, but the asymptotic value of B following the magnetic hole is not clear. In event 10 (Figure 5, right), data for the last part of the depression and the asymptotic value following it are not available. The Gaussian distribution provides a fit with $R^2 = 0.737$ for event 3 and $R^2 = 0.949$ for event 10. The widths of the magnetic holes are 1.83 ± 0.02 h and 2.28 ± 0.04 h, respectively. In event 3, B0 = 0.04 nT and B is very weak throughout, reaching the minimum value Bm = 0.02 nT, which is the uncertainty in each component of **B**. Consequently, near the minimum of the magnetic hole, the direction of **B** is not defined accurately, and there is a very large scatter of the 48 s averages of the angles. Within the uncertainties in the angles, the observations of the direction of **B** are consistent with a constant magnetic field direction. In event 10, the asymptotic magnetic fields are stronger, B0 = 0.12 nT and the minimum magnetic field is Bm = 0.05 nT, which is close to the 1 σ uncertainty in B, ±0.03 nT. For this event, there is increased variability in the 48 s averages where the magnetic fields are weak, and there is a small deviation in the magnetic field direction on a larger scale when the magnetic field is weak, owing to systematic errors manifesting themselves. Nevertheless, the data are consistent with the magnetic field direction being constant throughout the entire interval.

[38] There were two well-defined magnetic humps in the data set, which are shown in Figure 6. (The properties of these magnetic humps and a third magnetic hump are shown in Table 2. The center of the first magnetic hump (event 11, shown in Figure 6, left) moved past V1 at t_o = DOY 151.8781, and the center of the event 12 (shown in Figure 6, right) moved past V1 at t_o = DOY 308.1067. The first magnetic hump is well described by the Gaussian distribution. From this fit, we derive B0 = 0.03 nT, BM = 0.11 nT, and B0/BM = 0.26 nT, and the width w = 4.42 ± 0.06 h. Event 12, in Figure 6 (right), is less well defined. The Gaussian fit gives only $R^2 = 0.56$, with B0 = 0.12 nT, BM = 0.17 nT, B0/BM = 0.71 nT, and width w = 4.42 ± 0.06 h.

[39] The magnetic field direction for event 12 in Figure 6 (right) is remarkably constant, consistent with the relatively large fields throughout the interval (>0.12 nT) compared to the uncertainty in each component (±0.02 nT). In contrast, for event 11 in Figure 6 (left) the magnetic field direction is constant where B is close to 0.10 nT, but the direction of **B** changes and the fluctuations increase in magnitude approaching the weaker magnetic fields on either side of the magnetic hump, where the asymptotic values are 0.03 nT. These deviations can be attributed to the systematic and random errors in the measurements of the components.

4. Statistical Properties of the PBLs and the Magnetic Holes and Humps

[40] The basic parameters describing the magnetic field strength profile in the PBLs are the width of the current sheet w, and the magnetic field strengths before and after the current sheet (B1 and B2, respectively) that appear in equation (3). The basic parameters describing the magnetic field strength profile in a magnetic hole are the width w, the minimum magnetic field strength the magnetic hole Bm, and the magnetic field strength B0 before and after the magnetic depression. Finally, the basic parameters describing B(t) in a magnetic hump are the width w, the maximum

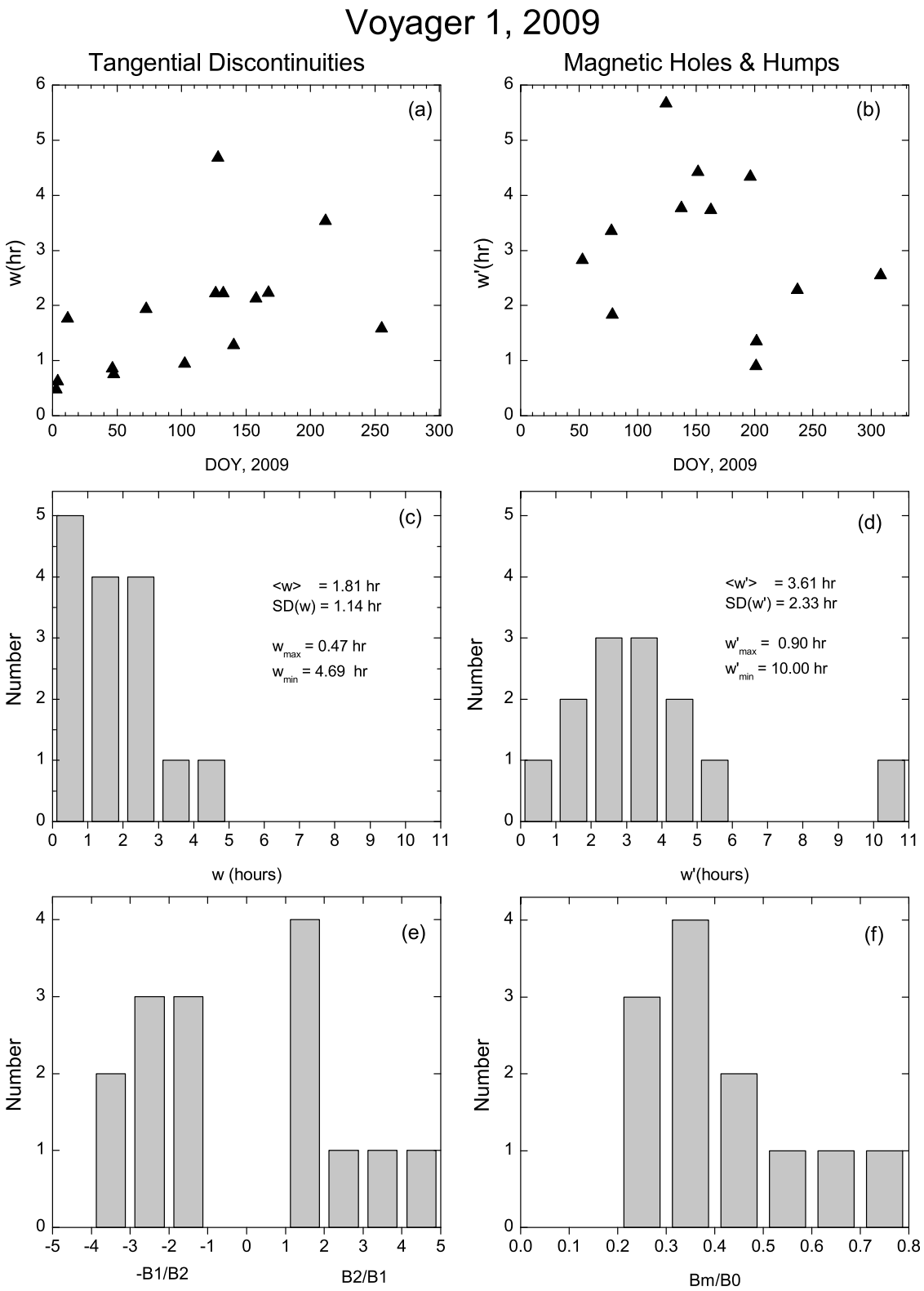

Figure 7. A comparison of the properties of (left) PBLs and (right) magnetic humps and holes. (a and b) The widths of the respective structures as a function of DOY. (c and d) The distribution of the widths (passage times) of the PBLs and the magnetic holes and humps, respectively. (e and f) T distributions of the extreme values of B in the PBLs and the magnetic holes and humps, respectively (see text).

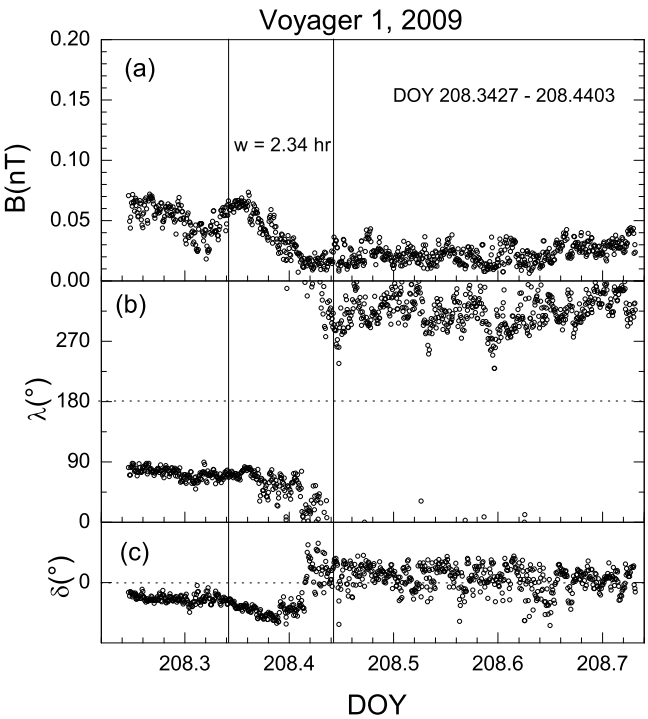

Figure 8. The observations of the current sheet associated with a sector boundary, plotted in the same format as the data and Figure 1.

magnetic field strength BM, and the field strength B0 before and after the magnetic hump. Of course, the time at which the structure moved past V1, t_o, must also be considered when fitting the data.

[41] The purpose of this section is to describe the statistical properties of the parameters for the PBLs as well as the magnetic holes and humps, and compare the parameters for these two types of structures. The statistical properties of the PBLs and the magnetic holes and humps were derived from the parameters in Tables 1 and 2, respectively. Data for the events in Tables 1 and 2 that are not in this paper can be found in the auxiliary material.

[42] The times at which the PBLs and the magnetic holes and humps were observed are shown in Figures 7a and 7b, respectively. One can see that both types of structures are distributed similarly in time throughout the 330 day interval. The widths of the PBLs as a function of the time t_0 that they move past V1 are plotted in Figure 7a. The widths of the magnetic holes and magnetic humps as a function of t_o are plotted in Figure 7b. Comparing Figures 7a and 7b, one can see that there is large variability in the widths of both types of structures. But the widths of the magnetic holes and humps tend to be larger than the widths of the PBLs.

[43] The average width (passage time) of PBLs is 1.81 h, and the average width of the magnetic holes and magnetic humps is 3.61 h. Thus, the width of the magnetic holes and magnetic humps is 2.0 times the width of the PBLs. The average width of linear magnetic holes observed by V1 in a unipolar region during 2006 [*Burlaga et al.*, 2007] was 2.3 ± 0.7 h, and the range of widths was from 1.2 to 3.4 h. The smaller passage time observed by V1 between DOYs 146 and 304, 2006 compared to 2009 could be related to the faster convection speed during 2006. The speed was V ≈ 80 km/s during 2006 and ~50 ± 20 km/s during 2009 [*Richardson*, 2011; R. B. Decker, private communication, 2010]. If we assume a constant thickness in kilometers, then we would infer that the average speed at V1 during 2009 is ~80 (km/s) × 2.3/3.6 ≈ 50 km/s, consistent with the results derived by the LECP team (see the review by *Richardson* [2011]).

[44] The widths of the PBLs range from 0.47 h to 4.69 h, and the widths of the magnetic holes and humps range from 0.90 h to 10.00 h. This would be expected if the magnetic holes and humps were planar structures with profiles resembling those of two PBLs side by side. (The Gaussian distribution that describes the magnetic holes and magnetic humps has two inflection points, while the sigmoid distribution that describes each of the PBLs has a single inflection point.) However, if magnetic holes are mirror mode structures with a sausage-like or a magnetic bottle shape, then one might expect the width to be relatively narrow near the neck of the bottle, and relatively broad near the center of the bottle. The distribution of the widths of the magnetic holes and humps should be broader than that for PBLs, which we did not observe. On the other hand, if the magnetic holes and humps have unidirectional magnetic fields and a nearly constant width along the magnetic field direction, then our results would be consistent with the passage of solitons.

[45] The distributions of the widths of the PBLs and of the magnetic holes and humps are shown in Figures 7c and 7d, respectively. The standard deviations of the widths of the PBLs and the magnetic holes and humps are 1.14 h and 2.33 h, respectively, differing by a factor 2. The distribution of the widths of the PBLs peaks between 0 and 1 h, and the distribution extends only from 0 to 5 h. In contrast, the distribution of the widths of the magnetic holes and humps peaks at ~3 h and the distribution extends from 0 to 11 h. The distributions show graphically and in more detail the sense in which the width, standard deviation, range of the widths for the magnetic holes and humps are twice that of the corresponding values for PBLs.

[46] As a measure of the size of the jumps of B across the PBLs, we use the ratios B2/B1 > 1 for "positive" jumps and B1/B2 < 1 for "negative" jumps. The distributions of these ratios are plotted in Figure 7e, where we plot −(B1/B2) for the negative jumps in order to separate the two distributions. It is apparent from Figure 7e that the number and magnitude of positive jumps is comparable to the number and magnitude of negative jumps, respectively.

[47] For the magnetic holes, the appropriate measure of the "amplitude" of the magnetic hole is Bm/B0, where Bm is the minimum value of the magnetic field strength of the magnetic hole and B0 is the magnetic field strength on either side. For the magnetic humps, the "amplitude" is BM/B0, where BM is the maximum magnetic field strength of the magnetic hump. Since there are only three magnetic humps in the data set, we include them in the distribution of amplitudes by substituting 1/(BM/B0) for BM/B0. The resulting distribution of Bm/B0 is shown in Figure 7f. There is a broad range of amplitudes, from 0.2 to 0.8, but the peak of the distribution of Bm/B0 is between 0.3 and 0.4, nearly a factor of 3 different from the ambient value. Nine of the

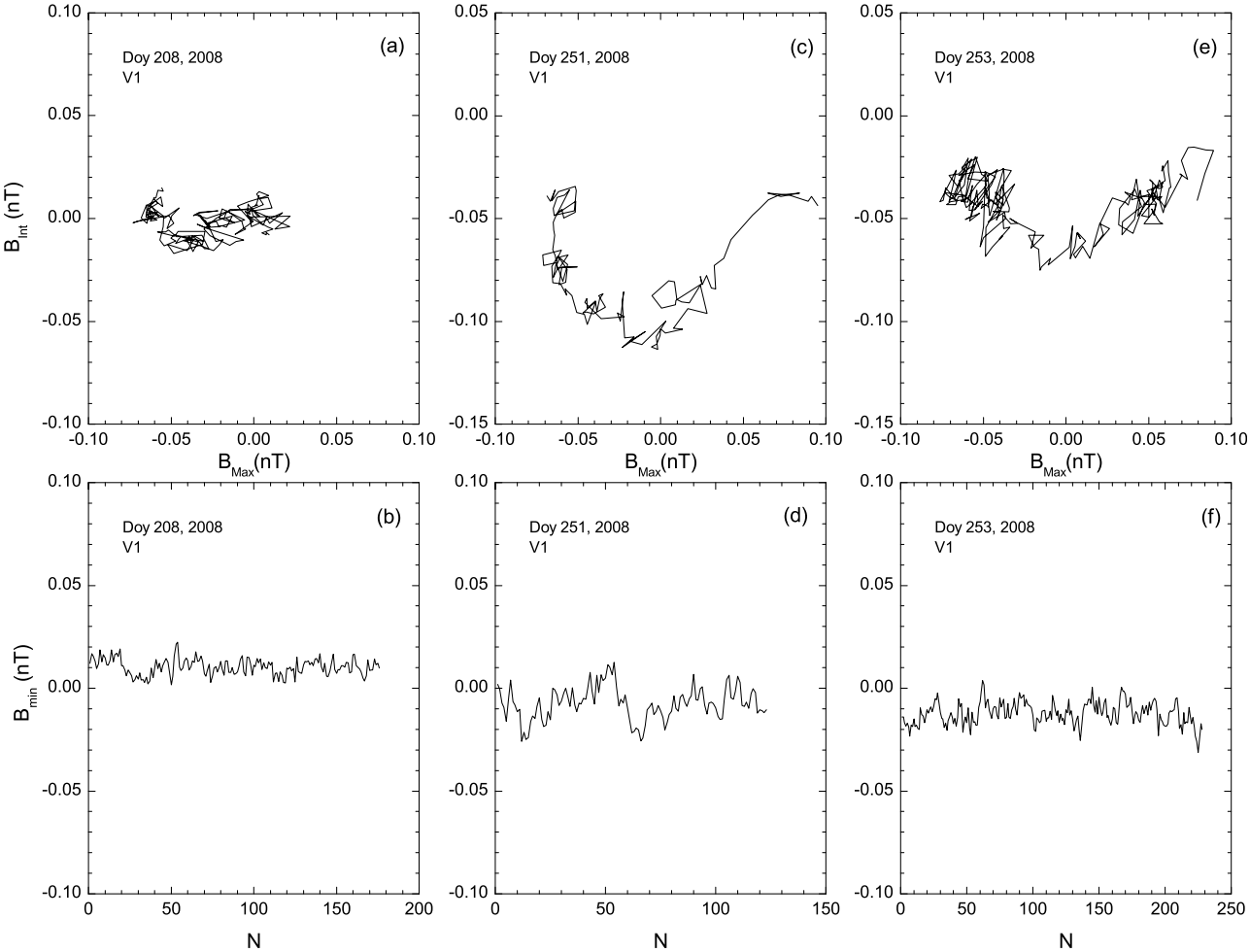

Figure 9. Hodograms produced by means of a minimum variance analysis for the current sheets associated with the sector boundaries in Figures 8 and 10. (b, d, and f) The value of the component of **B** along the minimum variance direction (Bm) as a function of time, N. (a, c, and e) The components of B along the intermediate variance direction (Bi) and maximum variance direction (BM).

13 events have Bm/B0 between 0.2 and 0.5, indicating significant (nonlinear) changes in B(t).

5. Current Sheets Associated With Sector Boundaries

[48] Several sector boundary crossings were observed by V1 from ~DOY 200, 2009 to DOY 255, 2009 (when V1 observed the extraordinary PBL which was the boundary of a large unipolar region with strong magnetic fields [*Burlaga and Ness*, 2010]. Unfortunately, we do not have data for most of these crossings, owing to data gaps and uncertainties in the measurements. Nevertheless, we have data for three sector boundaries, which are the subject of this section.

[49] A current sheet associated with a sector boundary moved past V1 from DOY 208.3421 to DOY 208.4403 is shown in Figure 8. It is obvious that the current sheet is neither a null sheet ("D sheet") nor a layer in which **B** with constant magnitude rotates through 180°. The magnetic field magnitude decreases across the current sheet from ~0.06 to 0.02 nT. There appears to be a small magnetic hole just before the arrival of the current sheet. Since B in the sector following the current sheet is near the limit of measurements, the angles in that sector cannot be determined accurately, which explains why the fluctuations in the angles are large and the change in the average angles before and after the sector boundary is not equal to 180°.

[50] The width of the current sheet associated with sector boundary on DOY 208 is ~2.34 h, which is close to the average width of the PBLs (1.81 h) discussed in section 2. Figure 8 shows that the angles change "smoothly" across the current sheet (apart from the large scatter 48 s averages which is associated with uncertainties in the measurements related to the weak magnetic fields). In general, the profile of B across a current sheet associated with a sector boundary is more complicated than those associated with the PBLs, but it is not a Harris current sheet [*Harris*, 1962].

[51] A minimum variance analysis of the data within the current sheet in Figure 8 gives the results shown in Figures 9a and 9b. The minimum variance direction in HG (RTN) coordinates is (1, 0, 0) with an uncertainty of at least ±0.03 in each of the components. Thus, the minimum variance direction is the radial direction. The

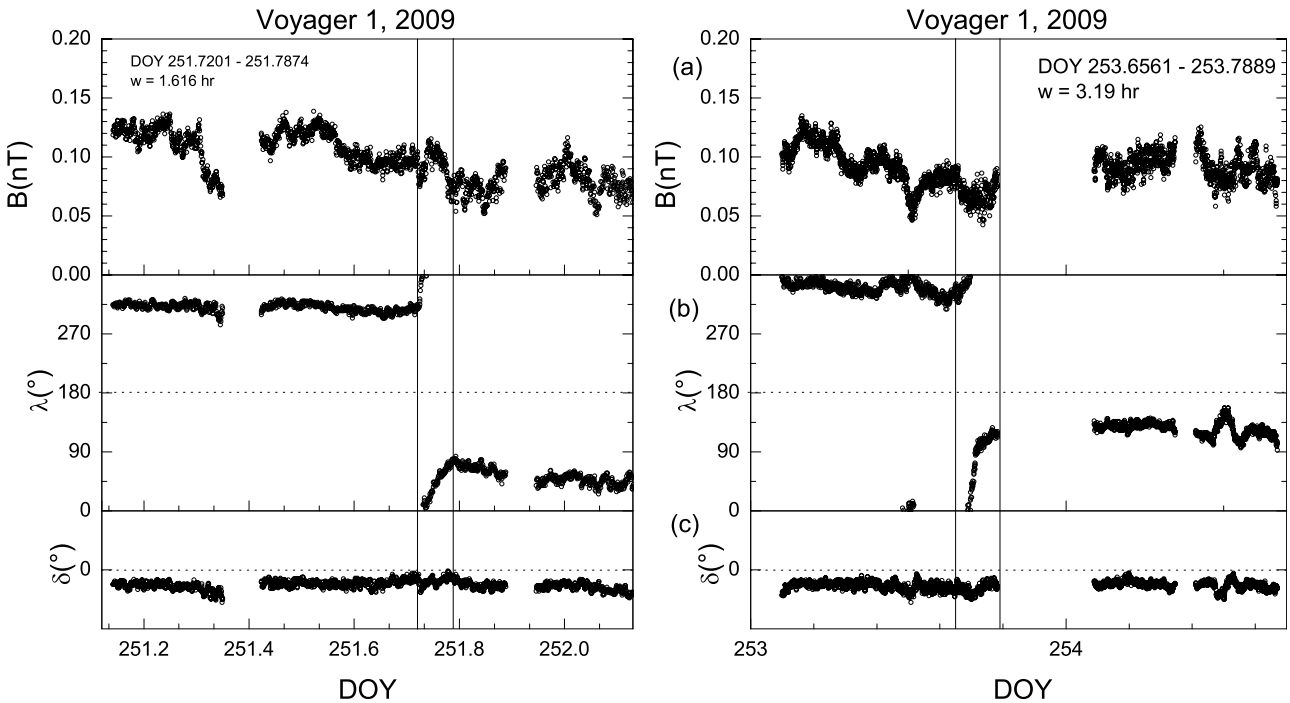

Figure 10. Observations of two current sheets, each associated with a sector boundary. The format is the same as that in Figure 1.

average component of **B** in the minimum variance direction is $B_{min} \approx 0.01$ nT (Figure 9b), which is consistent with 0 nT within the uncertainties. Thus, this sector boundary is a tangential discontinuity, and the plane of the discontinuity is approximately normal to the radial direction. The plot of the magnetic field components in the intermediate variance direction and the maximum variance direction, B_{Int} and B_{Max}, respectively (Figure 9a), shows a very shallow arc, because B was decreasing while **B** was rotating across the current sheet.

[52] Two additional current sheets were associated with the passage of sector boundaries past V1, on DOY 251 and DOY 253, shown in Figures 10 (left) and 10 (right), respectively. In both cases, the observations suggest that the direction of **B** does not change by 180° across the sector boundaries. However, the systematic uncertainty in the angles can be ±45°, even for magnetic fields of average strength, and larger for weaker magnetic fields. The current sheet associated with one of the sector boundaries moved past V1 from DOY 251.7201 to DOY 251.7872. The width of this current sheet was thus 1.62 h, which again is close to the average width for the PBLs (1.81 h). There was a small change in B across the current sheet, and there was small enhancement in B within the current sheet. Thus, the magnetic field strength profile is more complicated than that for the PBLs. The magnetic field direction changes nearly monotonically, primarily in the azimuthal direction, as shown in Figure 10 (left). The results of the minimum variance analysis for this current sheet are shown in Figure 9c. A plot of the components of **B** in the intermediate variance direction (B_{Int}) and maximum variance direction (B_{Max}), which define the "minimum variance plane") for the sector boundary on DOY 253 (Figure 9c), shows that the component of **B** in the minimum variance plane varies nearly along a circular arc across the current sheet. The minimum variance direction is (0.29, 0.07, 0.96), which is close to the N direction in HG coordinates, indicating a rotation primarily in the azimuthal direction. The component of **B** in the minimum variance direction fluctuates about zero throughout the event (Figure 9d), indicating that this current sheet is associated with the tangential discontinuity.

[53] Finally, we discuss a sector boundary observed by V1 DOY 253, 2009, shown in Figure 10 (right). In this case, the magnetic field direction is not close to the nominal Parker spiral field direction (270°/90°) on either side of the sector boundary, which may be a manifestation of the systematic uncertainties in the measurements. Nevertheless, there is a large change in the direction of **B** and it is reasonable to identify this change with a sector boundary. The magnitude of **B** is variable on both sides of the current sheet, and there is a slight depression within the current sheet. The current sheet moved past V1 from DOY 253.6561 to 253.79, giving a width of 3.19 h, which is larger than the average value for a PBLs but still within the range of the distribution of widths of PBLs (Figure 7c).

[54] The direction of **B** in this current sheet changes primarily in the azimuthal direction, as shown in Figure 10 (right). The minimum variance direction is given by the vector (0.40, 0.33, 0.83). The component of the **B** along the minimum variance direction (B_{Min}) fluctuates ~0.01 nT (Figure 9f), which is consistent with zero within the uncertainties. Once again, we find that the current sheet in the sector boundary is associated with a tangential discontinuity. The component of **B** in the plane of the tangential discontinuity (the minimum variance plane, normal to the mini-

mum variance direction) rotates about an elliptical arc (Figure 9e).

6. Thickness of the Current Sheets

[55] We have obtained the "widths" of current sheets associated with PBLs, magnetic holes and humps and current sheet associated with sector boundaries. These widths are actually passage times of the structures moving past V1. The quantity of physical interest is the geometrical thickness or the scale length of each of these structures.

[56] In order to derive a length from the time, one must know both the basic geometry of each class of structures and the velocity of the flow in the heliosheath relative to the velocity of V1. Since these parameters are not well known, we can only give order of magnitude estimates of the thickness of the current sheets, which illustrate the factors that must be considered.

[57] It is likely that the geometry of the PBLs and the current sheets associated with sector boundaries is locally a slab geometry, with a very large radius of curvature in the two principal directions at each point. In this case, the length of interest is the thickness of the slab. The geometry of isolated magnetic holes and humps in the heliosheath is not known. Since we found that the characteristic passage time of a magnetic hole or hump is twice that of a PBL or sector boundary, one needs to consider the possibility that the geometry of the observed magnetic holes and humps is locally that of a slab. On the other hand, the geometry of magnetic holes and humps might be tubular and sausage-like, with a different radius of curvature in each of the two principal directions at each point, varying along the axial direction. If the relevant geometry is that of a slab, then one must also know the orientation of the normal to the slab in order to derive its thickness. If the relevant geometry is tubular, then the measured thickness will depend on the orientation of the axis of the tube and the impact parameter with respect to the axis. Unfortunately, these parameters cannot be determined from measurements made by a single spacecraft such as V1.

[58] When the geometry is locally like that a slab, **B** is parallel to the surface of the slab and thus perpendicular to its normal. For the PBLs and magnetic holes and humps, the magnetic field direction (where it could be measured accurately) was nearly along the Parker magnetic field direction, with $\delta \approx 0°$ and $\lambda \approx 90°$ or 270°, and it did not vary significantly across the current sheet. Thus, the normal to a slab was in the meridional plane and inclined at an angle α relative to the **R** − **T** plane, which was not determined. We shall assume that $\alpha \approx 0°$, giving an upper limit on the thickness. Thus, we assume that the unit normal vector to a planar structure is **n** = **R** + **N** in the HG coordinates system. If the magnetic holes and humps are localized tubular structures, then the axis of the tube is close to the observed magnetic field direction, which is along the Parker spiral field direction.

[59] The determination of the velocity of the structures is also difficult. It is reasonable to assume that the PBLs and sector boundaries are convected with the heliosheath flow, so that their velocity relative to the flow is zero. Likewise, most theories suggest that the propagation speed of the slow mode waves associated with mirror structures or with solitons is negligible. Thus we shall assume that all of the structures move with the local velocity of the heliosheath. Unfortunately, the plasma instrument on V1 is not operating, but estimates of two components of the velocity (the radial and azimuthal components, WR and WT, respectively) were obtained by the LECP instrument team [*Richardson*, 2011; R. B. Decker, private communication, 2010]. For V1 during 2009, VR ≈ 20 km/s and VT ≈ −40 km/s, giving a speed in the RT plane of 45 km/s, with an uncertainty of ±15–20 km/s. In the absence of measurements of VN, we shall assume that VN ≈ 40 km/s. The speed of V1 is ~17 km/s in the radial direction. From the above numbers, we obtain an order of magnitude estimate for the velocity of plasma in the heliosheath relative to V1, $\mathbf{V_p}$ (km/s) ≈ 3 **R** − 40 **T** + 40 **N**. Note that the bulk velocity of flow in the heliosheath at the distance of V1 is not radial.

[60] If the thickness of a planar structure is L(km), its normal is **n**, and its velocity relative to V1 is $\mathbf{V_p}$, then the time for it to move past V1 is τ(s) ≈ L/[(**R** + 0 **T** + **N**) · (3**R** − 40 **T** + 40 **N**) = L/[3 + 40] = L(km)/43(km/s). Note that the thickness estimate depends primarily on the flow speed in the **N** direction and the inclination of the normal to the plane to the RT plane (assumed to be 0°) (since **B** is observed to be perpendicular to **N** and **R** for PBLs). We conclude that the maximum thickness of a planar structure is of the order of L (km) ≈ 43(km/s) × τ (s).

[61] Since the gyration of protons about the magnetic field direction is a key factor in determining the currents in the current sheets, the thickness of the current sheets may be expressed in terms of the proton gyroradius, $R_L = mcV_p/qB$, where m is the proton mass, q is the proton charge, B is the magnetic field strength, and V_p is the component normal to **B** of the velocity of the particle gyrating about **B**. From the distribution of pressure p as a function of energy in the heliosheath (including solar wind particles and pickup protons), G. Gloeckler (private communication, 2010) estimates the average temperature is T = p/nk ≈ 4.6 × 10^6 K. Then a gyrating particle (with 2 degrees of freedom) has V_p ≈ 195 km/s and, in a magnetic field with B ≈ 0.1 nT, the Larmor radius of the particle is R_L ≈ 18,500 km.

[62] For the PBLs, $\langle\tau\rangle$ = 1.8 h = 6500 s; hence, the order of magnitude of the thickness of the PBL is L_{PBL} = L = 43(km/s) × τ(s) = 300,000 km. If the characteristic Larmor radius is 18,500 km, then the order of magnitude of L_{PBL} is 15 R_L. *Burlaga et al.* [1977] found that the average thickness of tangential discontinuities at 1 AU was 1300 km = 12 R_L. Thus, the thickness of the PBLs in heliosheath at ~110 AU (where the thermal energy is dominated by energetic pickup protons) is comparable to the thickness of TDs at 1 AU (where the thermal energy is dominated by solar wind protons). The thicknesses of the PBLs derived from the theory of *Lemaire and Burlaga* [1976] range from 2 to 10 R_L. Thus, our observations of current sheets in the heliosheath which we identified as PBLs are consistent with this theory.

[63] If the magnetic holes and humps are tubular, with diameter (thickness) L_{mh} (km), and if the axis is in the Parker field direction **a** = **T**, then the maximum time for a magnetic hole or hump to move past V1 is τ_{mh} (s) = L_{mh}/[(**R** + 0 **T** + 0 **N**)·(3 **R** − 40 **T** + 40 **N**) = L_{mh}/3. For the magnetic holes and humps, $\langle\tau_{mh}\rangle$ = 3.6 h = 13,000 s. Hence, the order of magnitude of L_{mh} for tubular structures

is L_{mh}(km) < 3 km/s) × τ(s) = 36,000 km, and L_{mh} < 2 R_L, depending on the impact parameter. On the other hand, if magnetic holes and humps in heliosheath are 1-D solitons, as in the models of *Baumgärtel* [1999] and *Avinash and Zank* [2007], rather than sausage-like mirror mode structures, then one might model them as approximately two adjacent PBLs. In this case the thickness is of the order of L_{mh} = $2L_{PBL}$, consistent with our observation that the average width of the magnetic holes and humps is twice that of the PBLs. In this case the thickness of the solitons is of the order of L_{mh} = $2L_{PBL}$ ≈ 2 × 43(km/s) × τ_{mh} (s) ≈ 600,000 km = 30 R_L.

[64] The thickness of the current sheets associated with sector boundaries is well defined in principle, since the observations show that the three sector boundaries analyzed in this paper are tangential discontinuities. The normal to these discontinuities is the minimum variance direction. For the three sector boundaries shown in Figure 9 (on DOY 208, 251, and 253, 2009), the minimum variance directions are (1, 0, 0), (0.29, 0.03, 0.96), and (0.40, 0.33, 0.85) in HG coordinates, respectively. The normal of the sector boundary observed on DOY 208 was along the radial direction, but the normals of the sector boundaries on DOY 251 and 253 are highly inclined with respect to the radial direction, 74° and 58°, respectively. However, the uncertainties in these numbers are large, because the systematic errors are large owing to the relatively weak magnetic field strengths and because several operations on the components of **B** are involved in the computation of the minimum variance direction. It is likely that the uncertainty in the angles of the normals of the discontinuities is at least ±45°. The passage times of the three sector boundaries on DOY 208, 251, and 253 are 2.3, >3.2, and 1.6 h, respectively. Thus, without going to the details, it is clear that the thickness of the current sheets associated with sector boundaries is of the same order as the thickness of the PBLs.

7. Summary

[65] This paper examines the properties of current sheets associated with proton boundary layers ("PBLs"), magnetic holes and humps, and sector boundaries observed deep in the heliosheath by Voyager 1 DOY 1–331, 2009 between 108.5 and 111.8 AU. We identified 15 PBLs, (corresponding to a rate of 0.096/d), 10 magnetic holes, 3 magnetic holes, and 3 sector boundaries in ~175 days of data during the 331 day interval.

[66] The PBLs were associated with increases and decreases in the magnetic field strength B(t) across the current sheet, in approximately equal numbers. The shape of B(t) can be described by a sigmoid function or equivalently a function involving the hyperbolic tangent. The magnetic field strength increases or decreases monotonically across the current sheet, with a single inflection point in the middle of the current sheet.

[67] The average "width" w (passage time) of the current sheets associated with PBLs is 1.81 h, and the standard deviation is 1.14 h. The widths of the PBLs range from 0.47 h to 4.69 h, and the distribution of widths is peaked between 0 and 1 h, with only two events with w between 3 and 5 h. Estimates of the velocity at which the PBLs were carried past V1 were obtained from estimates of the velocity in the heliosheath derived from the measurements of the LECP instrument. The average thickness L of the PBLs is of the order of 300,000 km. If the gyroradius is of the order 18,500 km, corresponding to an isotropic temperature of 4.6 × 10^6 K, then the order of magnitude of L is 15 R_L. This thickness in units of the Larmor radius is of the same order of magnitude as the thickness of the current sheets associated with tangential discontinuities observed at 1 AU [*Turner et al.*, 1977] and the thickness of PBLs predicted by the kinetic theory of *Lemaire and Burlaga* [1976]. The direction of the magnetic field did not change significantly in the PBLs. In most cases, the magnetic field direction was close to that of the Parker spiral magnetic field directions, δ = 0° and λ = 90° or 270°.

[68] Ten magnetic holes and three magnetic humps were identified in the V1 data from DOY 1–331, 2009. The predominance of magnetic holes may be related to the preferential production of magnetic holes and more rapid decay of magnetic humps. The observed ratio of magnetic holes to magnetic humps, 10/3, places a constraint on theories of the nature and evolution of magnetic holes and humps. As found in earlier observations of magnetic holes and humps in the heliosheath, their shapes can be described by fits to a Gaussian function. Although this function is not unique, it gives the correct qualitative profile of the current sheet (a smooth variation with single extremum and two inflection points), and it gives good estimates of the parameters describing the magnetic holes and humps.

[69] The average width of the magnetic holes and humps was 3.6 h, twice the average width of the current sheets associated with PBLs. On the one hand, this is not surprising, since the profile of a magnetic hole or hump resembles that of two PBLs, side by side. On the other hand, if the magnetic holes and humps are mirror mode structures, one might expect a broader distribution of widths; relatively thin structures would be observed by V1 when it passed through the neck of the magnetic bottle and relatively broad structures would be observed when V1 passed through the center of the bottle. The widths of the magnetic holes and humps range from 0.90 h to 10.00 h, approximately twice the range of widths for PBLs. The standard deviation of the widths of magnetic holes and humps is 2.33, approximately twice the value 1.14 observed for PBLs. The thickness of magnetic holes and humps is of the order of 600,000 km = 30 R_L., twice the thickness of PBLs. These numbers support the hypothesis that the magnetic holes and humps observed by V1 are planar structures, such as solitons.

[70] We identified three sector boundaries for which observations of the current sheets could be analyzed. In contrast to the PBLs discussed above (where there was no variation in the magnetic field direction), there was obviously a large change in the direction of the magnetic field across the sector boundaries. For each of the three sector boundaries, the magnetic field vector rotated in a plane normal to the minimum variance direction, and the component of the magnetic field along the minimum variance direction was zero within the uncertainties. This indicates that the sector boundaries were tangential discontinuities. The thickness of two of the current sheets associated with sector boundaries was very close to the average thickness of the current sheets associated with the PBLs that we ana-

lyzed, and the width of the current sheet associated with the third sector boundary was within the range of widths of the current sheets associated with PBLs that we discuss in section 2. However, the variations of B across the current sheets associated with the sector boundaries are more complicated than the corresponding profiles for the PBLs. We found no evidence for magnetic reconnection in the V1 data for 2009.

[71] In summary, all three types of current sheets resemble pressure balanced structures, but there are important differences. The current sheets associated with the sector boundaries discussed in section 5 and those associated with the isolated PBLs discussed in section 3 are probably planar structures. The magnetic field strength in the current sheet varies along the normal to the plane of the structure, and the direction of the magnetic field is parallel to the plane. These two types of structures have similar widths. However, the direction of **B** changes in sector boundaries but not in the isolated PBLs, and the magnetic field strength profiles across the sector boundaries are more complicated than those for PBLs.

[72] The direction of the magnetic fields associated with magnetic holes and humps did not change significantly as these structures moved past V1. The magnetic field strength in magnetic holes and humps might vary along the magnetic field direction, but we cannot determine this directly from the V1 observations. Instead, V1 sampled along a line across the magnetic holes and humps. We find no evidence for a magnetic bottle geometry associated with magnetic holes and humps. The direction of **B** is constant (within the uncertainties of the measurements), and there is no statistical evidence that V1 passed through unusually thin regions associated with the neck of a magnetic bottle or unusually thick regions associated with the center of magnetic bottle. Since even structures that evolved from the mirror mode instability would have a nearly constant pressure through this cross section, one might expect to observe smooth magnetic field strength profiles resembling those of two adjacent PBLs, having twice the width of a PBL, in agreement with our observations.

[73] Rather than debate whether the magnetic holes and humps are current sheets associated with PBLs described by Vlasov equation, mirror mode waves related to the mirror mode instability, or solitons, one should explore the hypothesis that all three of these characteristics are properties of magnetic holes and humps. In particular, motivated by recent theoretical studies, it would be interesting to test the hypothesis that magnetic holes and humps can be initiated by the mirror mode instability, evolve by nonlinear kinetic processes to solitons, that may or may not interact, and form isolated very slowly propagating pressure balanced structures maintained by the magnetization and gradient drift currents of protons in the inhomogeneous magnetic fields of the soliton. This test will require additional theoretical work, detailed relatively complete observations from more than one spacecraft.

[74] **Acknowledgments.** T. McClanahan and S. Kramer processed the data. Daniel Berdischevsky computed the zero level offsets for the instrument for the data. N. F. Ness was partially supported in part by NASA grant NNX09AT41G to CUA.

[75] Philippa Browning thanks Joseph Lemaire and another reviewer for their assistance in evaluating this paper.

References

Avinash, K., and G. P. Zank (2007), Magnetic structures in the heliosheath, *Geophys. Res. Lett.*, *34*, L05106, doi:10.1029/2006GL028582.

Avinash, K., S. M. Cox, D. Shaikh, and G. P. Zank (2009), Four-fluid model and numerical simulations of magnetic structures in the heliosheath, *Astrophys. J.*, *695*, 420–430, doi:10.1088/0004-637X/695/1/420.

Baumgärtel, K. (1999), Soliton approach to magnetic holes, *J. Geophys. Res.*, *104*, 28,295–28,308, doi:10.1029/1999JA900393.

Baumgärtel, K., E. Dubinin, K. Sauer, and T. Story (1997), Solar wind magnetic holes: Signatures of slow-mode type MHD solitons, *Adv. Space Res.*, *20*, 69–74, doi:10.1016/S0273-1177(97)00483-3.

Baumgärtel, K., K. Sauer, and E. Dubinin (2005), Kinetic slow mode-type solitons, *Nonlinear Processes Geophys.*, *12*, 291–298, doi:10.5194/npg-12-291-2005.

Baumgärtel, K., K. Sauer, E. Mjølhus, and E. Dubinin (2007), Fluid versus simulation model of solitons in solar wind: Application to Ulysses observations, *J. Geophys. Res.*, *112*, A12101, doi:10.1029/2007JA012557.

Bavassano Cattaneo, M. B., C. Basile, G. Moreno, and J. D. Richardson (1998), Evolution of mirror structures in the magnetosheath of Saturn from the bow shock to the magnetopause, *J. Geophys. Res.*, *103*, 11,961–11,972, doi:10.1029/97JA03683.

Burlaga, L. F. (1968), Micro-scale structures in the interplanetary medium, *Sol. Phys.*, *4*, 67–92, doi:10.1007/BF00146999.

Burlaga, L. F. (1995), *Interplanetary Magnetohydrodynamics*, Oxford Univ. Press, New York.

Burlaga, L. F., and J. F. Lemaire (1978), Interplanetary magnetic holes: Theory, *J. Geophys. Res.*, *83*, 5157–5160, doi:10.1029/JA083iA11p05157.

Burlaga, L. F., and N. F. Ness (1969), Macro- and micro-structure of the interplanetary magnetic field, *Can. J. Phys.*, *46*, S962–S965.

Burlaga, L. F., and N. F. Ness (2010), Sectors and large-scale magnetic field strength fluctuations in the heliosheath near 110 AU, Voyager 1, 2009, *Astrophys. J.*, *725*, 1306–1316, doi:10.1088/0004-637X/725/1/1306.

Burlaga, L. F., J. Lemaire, and J. M. Turner (1977), Interplanetary current sheets at 1 AU, *J. Geophys. Res.*, *82*, 3191–3200, doi:10.1029/JA082i022p03191.

Burlaga, L. F., N. F. Ness, and J. W. Belcher (1996), Pickup protons and pressure balanced structures from 39 to 43 AU: Voyager 2 observations during1993 and 1994, *J. Geophys. Res.*, *101*, 15,523–15,532, doi:10.1029/96JA01076.

Burlaga, L. F., N. F. Ness, M. H. Acuña, R. P. Lepping, J. E. P. Connerney, E. C. Stone, and F. B. McDonald (2005), Crossing the termination shock into the heliosheath: Magnetic fields, *Science*, *309*, 2027–2029, doi:10.1126/science.1117542.

Burlaga, L. F., N. F. Ness, and M. H. Acuña (2006a), Magnetic fields in the heliosheath: Voyager 1 observations, *Astrophys. J.*, *642*, 584–592, doi:10.1086/500826.

Burlaga, L. F., N. F. Ness, and M. H. Acuña (2006b), Trains of magnetic holes and magnetic humps in the heliosheath, *Geophys. Res. Lett.*, *33*, L21106, doi:10.1029/2006GL027276.

Burlaga, L. F., N. F. Ness, and M. H. Acuña (2007), Linear magnetic holes in a unipolar region of the heliosheath observed by Voyager 1, *J. Geophys. Res.*, *112*, A07106, doi:10.1029/2007JA012292.

Burlaga, L. F., N. F. Ness, M. H. Acuña, R. P. Lepping, and J. E. P. Connerney (2008), Observations of magnetic fields at the solar wind termination shock, *Nature*, *454*, 75–77, doi:10.1038/nature07029.

Burlaga, L. F., N. F. Ness, M. H. Acuña, J. D. Richardson, E. Stone, and F. B. McDonald (2009), Observations of the heliosheath and solar wind near the termination shock by Voyager 2, *Astrophys. J.*, *692*(2), 1125–1130, doi:10.1088/0004-637X/692/2/1125.

Constantinescu, O. D., K.-H. Glassmeier, R. Treumann, and K.-H. Fornaçon (2003), Magnetic mirror structures observed by Cluster in the magnetosheath, *Geophys. Res. Lett.*, *30*(15), 1802, doi:10.1029/2003GL017313.

Erdös, G., and A. Balogh (1996), Statistical properties of mirror mode structures observed by Ulysses in the magnetosheath of Jupiter, *J. Geophys. Res.*, *101*, 1–12, doi:10.1029/95JA02207.

Fitzenreiter, R. J., and L. F. Burlaga (1978), Structure of sheets in magnetic holes at 1 AU, *J. Geophys. Res.*, *83*, 5579–5585 doi:10.1029/JA083iA12p05579.

Génot, V., S. J. Schwartz, C. Mazelle, M. Balikhin, M. Dunlop, and T. M. Bauer (2001), Kinetic study of the mirror mode, *J. Geophys. Res.*, *106*, 21,611–21,622, doi:10.1029/2000JA000457.

Génot, V. (2008), Mirror and firehose instabilities in the heliosheath, *Astrophys. J.*, *687*, L119–L122, doi:10.1086/593325.

Hall, A. N. (1979), Finite ion Larmor radius modifications to the firehose and mirror instabilities, *J. Plasma Phys.*, *21*, 431–443, doi:10.1017/S0022377800022005.

Harris, E. G. (1962), On a plasma sheath separating regions of oppositely directed magnetic fields, *Nuovo Cim.*, *23*, 115–121, doi:10.1007/BF02733547.

Hasegawa, A. (1969), Drift mirror instability in the magnetosphere, *Phys. Fluids*, *12*, 2642, doi:10.1063/1.1692407.

Horbury, T. S., E. A. Lucek, A. Balogh, I. Dandouras, and H. Rème (2004), Motion and orientation of magnetic field dips and peaks in the terrestrial magnetosheath, *J. Geophys. Res.*, *109*, A09209, doi:10.1029/2003JA010237.

Istomin, Y. N., O. A. Pokhotelov, and M. A. Balikhin (2009), Mirror instability in space plasmas: Solitons and cnoidal waves, *Phys. Plasmas*, *16*, 062905, doi:10.1063/1.3153553.

Joy, S. P., M. G. Kivelson, R. J. Walker, K. K. Khurana, C. T. Russell, and W. R. Paterson (2006), Mirror mode structures in the Jovian magnetosheath, *J. Geophys. Res.*, *111*, A12212, doi:10.1029/2006JA011985.

King, J. H., K. W. Ogilvie, and K. W. Behannon (1979), Plasma electron observations in the vicinity of magnetic holes, *J. Geophys. Res.*, *84*, 5333–5338, doi:10.1029/JA084iA09p05333.

Kivelson, M. G., and D. J. Southwood (1996), Mirror instability: 2. The mechanism of nonlinear saturation, *J. Geophys. Res.*, *101*, 17,365–17,371, doi:10.1029/96JA01407.

Klein, L. W., and L. F. Burlaga (1980), Interplanetary sector boundaries 1971–1973, *J. Geophys. Res.*, *85*, 2269–2276, doi:10.1029/JA085iA05p02269.

Korteweg, D. J., and G. de Vries (1895), On the change of form of long waves advancing in a rectangular canal and on a new type of long stationary waves, *Philos. Mag.*, *39*(240), 422–443.

Lamb, G. L. (1980), *Elements of Soliton Theory*, Wiley-Interscience, Hoboken, N. J.

Levenberg, K. (1944), A method for the solution of certain problems in least squares, *Q. Appl. Math.*, *2*, 164–168.

Lemaire, J., and L. F. Burlaga (1976), Diamagnetic boundary layers: A kinetic theory, *Astrophys. Space Sci.*, *45*, 303–325, doi:10.1007/BF00642667.

Liu, Y., J. D. Richardson, J. W. Belcher, J. C. Kasper, and R. M. Skoug (2006), Plasma depletion and mirror waves ahead of interplanetary coronal mass ejections, *J. Geophys. Res.*, *111*, A09108, doi:10.1029/2006JA011723.

Marquardt, D. (1963), An algorithm for least-squares estimation of nonlinear parameters, *SIAM J. Appl. Math.*, *11*, 431–441, doi:10.1137/0111030.

Neugebauer, M., B. E. Goldstein, D. Winterhalter, E. J. Smith, R. J. MacDowall, and S. P. Gary (2001), Ion distributions in large magnetic holes in the fast solar wind, *J. Geophys. Res.*, *106*, 5635–5648, doi:10.1029/2000JA000331.

Pantellini, F. G. E. (1998), A model of the formation of stable nonpropagating magnetic structures in the solar wind based on the nonlinear mirror instability, *J. Geophys. Res.*, *103*, 4789–4798, doi:10.1029/97JA02384.

Pokhotelov, O. A., R. Z. Sagdeev, M. A. Balikhin, and R. A. Treumann (2004), Mirror instability finite ion-Larmor radius wavelengths, *J. Geophys. Res.*, *109*, A09213, doi:10.1029/2004JA010568.

Pokhotelov, O. A., R. Z. Sagdeev, M. A. Balikhin, O. G. Onishchenko, and V. N. Fedun (2008), Nonlinear mirror waves in non-Maxwellian space plasmas, *J. Geophys. Res.*, *113*, A04225, doi:10.1029/2007JA012642.

Rees, A., A. Balogh, and T. S. Horbury (2006), Small-scale solitary wave pulses observed by the Ulysses magnetic field experiment, *J. Geophys. Res.*, *111*, A10106, doi:10.1029/2005JA011555.

Richardson, J. D. (2011), Observations of the termination shock and heliosheath, in *The Sun, the Solar Wind, and the Heliosphere*, *IAGA Spec. Sopron Book Ser.*, vol. 4, edited by M. P. Miralles and J. S. Almeida, Springer, New York, doi:10.1007/978-90-481-9787-3_13, in press.

Sauer, K., E. Mjølhus, E. Dubinin, and K. Baumgärtel (2007), Banana-polarized solitons in anisotropic plasma related to Ulysses observations, *Geophys. Res. Lett.*, *34*, L11109, doi:10.1029/2007GL029583.

Smith, E. J. (2001), The heliospheric current sheet, *J. Geophys. Res.*, *106*, 15,819–15,831, doi:10.1029/2000JA000120.

Soucek, J., E. Lucek, and I. Dandouras (2008), Properties of magnetosheath mirror modes observed by Cluster and their response to changes in plasma parameters, *J. Geophys. Res.*, *113*, A04203, doi:10.1029/2007JA012649.

Southwood, D. J., and M. G. Kivelson (1993), Mirror instability: 1. Physical mechanism of linear instability, *J. Geophys. Res.*, *98*, 9181–9187, doi:10.1029/92JA02837.

Sperveslage, K., F. M. Neubauer, K. Baumgärtel, and N. F. Ness (2000), Magnetic holes in the solar wind between 0.3 AU and 17 AU, *Nonlinear Processes Geophys.*, *7*, 191–200, doi:10.5194/npg-7-191-2000.

Stasiewicz, K., P. K. Shukla, G. Gustafsson, S. Buchert, B. Lavraud, B. Thide, and Z. Klosv (2003), Slow magnetosonic solitons detected by the Cluster spacecraft, *Phys. Rev. Lett.*, *90*(8), 085002, doi:10.1103/PhysRevLett.90.085002.

Stevens, M. L., and J. C. Kasper (2007), A scale-free analysis of magnetic holes at 1 AU, *J. Geophys. Res.*, *112*, A05109, doi:10.1029/2006JA012116.

Stone, E. C., A. C. Cummings, F. B. McDonald, B. C. Heikkila, N. Lal, and W. R. Webber (2005), Voyager 1 explores the termination shock region and the heliosheath beyond September 2005, *Science*, *309*, 2017–2020, doi:10.1126/science.1117684.

Stone, E. C., et al. (2008), Voyager 2 finds an asymmetric termination shock and explores the heliosheath beyond, *Nature*, *454*, 71–74, doi:10.1038/nature07022.

Tajiri, M. (1967), Propagation of magnetohydrodynamic waves in collisionless plasmas, II, Kinetic approach, *J. Phys. Soc. Jpn.*, *22*, 1482–1494, doi:10.1143/JPSJ.22.1482.

Tátrallyay, M., and G. Erdös (2002), The evolution of mirror mode fluctuations in the terrestrial magnetosheath, *Planet. Space Sci.*, *50*, 593–599, doi:10.1016/S0032-0633(02)00038-7.

Tátrallyay, M., and G. Erdös (2005), Statistical investigation of mirror type magnetic field depressions observed by ISEE-1, *Planet. Space Sci.*, *53*, 33–40, doi:10.1016/j.pss.2004.09.026.

Tsurutani, B. T., D. Southwood, E. J. Smith, and A. Balogh (1992), Nonlinear magnetosonic waves and mirror mode structures in the March 1991 Ulysses interplanetary event, *Geophys. Res. Lett.*, *19*, 1267–1270, doi:10.1029/92GL00782.

Tsurutani, B. T., C. Galvan, J. K. Arballo, D. Winterhalter, R. Sakurai, E. J. Smith, B. Buti, G. S. Lakhina, and A. Balogh (2002), Relationship between discontinuities, magnetic holes, magnetic decreases, and nonlinear Alfvén waves: Ulysses observations over the solar poles, *Geophys. Res. Lett.*, *29*(11), 1528, doi:10.1029/2001GL013623.

Tsurutani, B. T., G. S. Lakhina, O. P. Verkhoglyadova, E. Echer, F. L. Guarnieri, Y. Narita, and D. O. Constantinescu (2011), Magnetosheath and heliosheath mirror mode structures, interplanetary magnetic decreases, and linear magnetic decreases: Differences and distinguishing features, *J. Geophys. Res.*, *116*, A02103, doi:10.1029/2010JA015913.

Turner, J. M., L. F. Burlaga, N. F. Ness, and J. F. Lemaire (1977), Magnetic holes in the solar wind, *J. Geophys. Res.*, *82*, 1921–1924, doi:10.1029/JA082i013p01921.

Winterhalter, D., M. Neugebauer, B. E. Goldstein, E. J. Smith, S. Bame, and A. Balogh (1994a), ULYSSES field and plasma observations of magnetic holes in the solar wind and their relation to mirror-mode structures, *J. Geophys. Res.*, *99*, 23,371–23,381, doi:10.1029/94JA01977.

Winterhalter, D., E. J. Smith, M. E. Burton, N. Murphy, and D. J. McComas (1994b), ULYSSES field and plasma observations of magnetic holes in the solar wind and their relation to mirror-mode structures, *J. Geophys. Res.*, *99*, 6667–6680, doi:10.1029/93JA03481.

Winterhalter, D., E. J. Smith, M. Neugebauer, B. E. Goldstein, and B. T. Tsurutani (2000), The latitudinal distribution of solar wind magnetic holes, *Geophys. Res. Lett.*, *27*, 1615–1618, doi:10.1029/1999GL003717.

L. F. Burlaga, Geospace Physics Laboratory, Code 673, NASA Goddard Space Flight Center, Greenbelt, MD 20771, USA. (lburlagahsp@verizon.net)

N. F. Ness, Institute for Astrophysics and Computational Sciences, Catholic University of America, Washington, DC 20064, USA. (nfnudel@yahoo.com)